

Received January 21, 2021, accepted February 4, 2021, date of publication February 8, 2021, date of current version February 17, 2021.

Digital Object Identifier 10.1109/ACCESS.2021.3057931

FESD: An Approach for Biometric Human Footprint Matching Using Fuzzy Ensemble Learning

SHAKILA BASHEER¹, KAPIL KUMAR NAGWANSHI², (Senior Member, IEEE),
SURBHI BHATIA³, SIPI DUBEY⁴, AND G. R. SINHA⁵, (Senior Member, IEEE)

¹Department of Information Systems, College of Computer and Information Sciences, Princess Nourah bint Abdulrahman University, Riyadh 11564, Saudi Arabia

²Department of Computer Science and Engineering, Amity University Rajasthan, Jaipur 302006, India

³Department of Information Systems, College of Computer Science and Information Technology, King Faisal University, Hofuf 31982, Saudi Arabia

⁴Department of Computer Science and Engineering, RCET Bhilai, CSVTU Bhilai, Bhilai 491107, India

⁵Department of Electronics and Communication Engineering, Myanmar Institute of Information Technology, Mandalay 05072, Myanmar

Corresponding author: Kapil Kumar Nagwanshi (dr.kapil@ieee.org)

This research was funded by the Deanship of Scientific Research at Princess Nourah bint Abdulrahman University through the Fast-track Research funding program.

ABSTRACT Biometric traits such as fingerprint, retina scan, and palm-prints are used to identify a person at attendance monitoring, banking, passport, travel, and many other applications. Biometric-based person identification is the only method that never changes according to time, and no one can copy it without knowledge. Footprint-based biometric is one way to recognize a person based on different features associated with human footprints. For example, some places, such as airports, nanotechnology laboratories, silicon industries, temples, and public areas, require high security. It is necessary to add a footprint-based biometric trait for such high alert areas. The number of subjects taken by existing footprint-based methods is limited to very few subjects. The above research gaps motivate to add more subjects for this study. The proposed algorithm utilizes the fuzzy logic-based method for personal identification. Considerably 220 subjects with temporal aspects are taken into account to fill the existing methods gap. Three approaches, Fine Gaussian SVM (FSVM), Fine KNN (FKNN), and Fuzzy Ensemble Subspace Discriminant (FESD), have been utilized to create the enhanced human footprint matcher. The Fine Gaussian SVM approach exhibits an accuracy of 84.7%, the FKNN approach results in an accuracy of 92.3%, and the FESD approach gives an accuracy of 98.89%. FESD approach rectifies the recognition rate (to reach the required accuracy of 98.88%) False Match Rate (FMR, the rate of falsely as genuine classified imposters) at 0.01, False Non-Match Rate at 0.093 which is the rate of falsely as imposter classified genuine users) to a set of different matchers for the identification task. It improves the speed of recognition with 220 subjects by implementing the prototype schemes for footprint biometric to evaluate system properties, including accuracy and performance.

INDEX TERMS Biometric, ensemble, fuzzy logic, FDR, FNMR, FRR, footprint, KNN, SVM.

I. INTRODUCTION

There are many biometric matching techniques available for identification. Footprint-based biometric is a considerably newer technique for personal identification. Some other methods based on smart cards are also available. One can easily intrude the methods based on smart cards. Most of the means for personal identification are used for attendance

The associate editor coordinating the review of this manuscript and approving it for publication was Guitao Cao¹.

monitoring. The footprint-based matching technique does not propose it as a method for attendance monitoring though it has the capability for the same. In cases where a person without hands can use this technique for attendance monitoring. Aadhar in India is such a card that stores biometric data of face, retina, palm, and fingers but not the footprint [1]–[4].

The footprint-based is implemented due to its importance in many instances of the crime scene where an accused must walk around and left the footwear impressions as well as bare-foot prints and therefore it is very crucial to recovering the

footprints to identify criminals. Nowadays, terrorist attacks are so frequent and become a significant challenge for the country and society. Industries for example defense organizations, pharmaceutical, silicon chip manufacturing units, nanotechnology industries, religious places such as temples, public areas, market, shops are the soft targets for terrorists. Naples [5] presented an analysis of foot and footwear characteristics, impressions, and trackways that lead to significant evidence in a crime scene investigation.

A. RELATED WORK

Nakajima *et al* [6] developed a BIG-MAT sensor system to capture the impression of a footprint. They have arranged 110 samples from 10 subjects. Later, the pressure mat using Hidden Markov Model combined the Levenberg-Marquart learning method proposed by Jung *et al* [7]–[10], and Yun *et al* [11], which gives a recognition rate of 64% to 80% from among 11 samples. Uhl and Wild [12], [13] developed a method based on Eigenfeet, ball-print and foot geometry biometrics for 16 subjects with a recognition rate of 97%. One application of human footprint is estimating stature from footprint and foot outline dimension for crime background identification. In this regard, Krishnan [14] has applied his analysis among 1040 males between 18 years to 30 years. This method is intended to find foot geometry for the identification of criminals. A similar kind of study has completed by Moorthy and Sulaiman [15] for Malay persons for 400 persons. Despite of manual work, this analysis gives a direction for the forensic examination of a crime scene. Takeda *et al* [16]–[18] implemented a fuzzy-logic-based solution using a load distribution sensor from 30 subjects. The EER observed using this method was 6.1 % and FRR of 13.9 %. Ye *et al* [19] presented a method based on ANN amidst a similar pressure sensor mat with 11 volunteers. Here FRR varies from 28.6 % to 12 % with lesser subjects. The study on a wavelet and fuzzy-neural network for footprint has carried out by Wang *et al* [20] with a recognition rate of 92.8 % from 80 toe images.

Later on, MSHET was introduced by Kumar and Ramakrishnan [21] for 400 subjects with a 92% recognition rate, but no dataset has been produced. Kumar and Shekhar [22] developed a multibiometrics rank-level fusion system for palm and foot with a claim of using palmprints from 517 subjects and suggested an accuracy of 92-99% using fusion. Pataky [23] used 1040 dynamic foot pressure images from 10 volunteers, and due to the high correlation between images, the accuracy obtained was 99%. The discrete correlation of footprint image presented by Kumar *et al* [24]–[26] gives a general framework for the footprint-based system. Fernandez has explained the use of footprint to identify newborn babies where multiple births occur with the highest recognition rate of 96%. Kumar and Ramakrishnan [27] elaborated PCA and ICA based method, where 21 subjects will give a recognition rate of 95.24%. Hashem and Ghali [28] used ANN for 40 subjects with a 92% recognition rate.

B. MOTIVATION

This work has motivated by the gap analysis presented by Nagwanshi in [39]. According to the study presented in Table 1, the number of subjects taken by other footprint based methods is limited to very few, which is motivated to add more subjects. The human foot-based identification method includes the gait, footprint, and shoes of a person. Personal identification using behavioral patterns of gait is challenging as the volume of data required is very high. The footwear also not sufficient for the identification of a person. The existing footprint-based method results in degradation of performance while adding more subjects. This work also motivates creating a large dataset, and creating a dataset is also a very challenging task. The next motivating factor is to rectify the match rate to reach the required accuracy of 98%. Ascertain the employability of the footprint concerning temporal and physical features is another encouraging factor. And the final motivating factor is to improve the speed of recognition with beyond 200 subjects; and implement the prototype schemes for footprint biometric to evaluate system properties, including accuracy and performance; and promotes it to install in legal capacities to identify the person or impostor [37], [40]–[43].

II. MATERIALS

The materials used for implementation of footprint-based matcher include hardware resources, the operating system, tools and publication of data-set. Each of these has described as follows.

A. HARDWARE RESOURCES

The experimental system is configured with Intel Core i5 2430M 2.4 GHz dual core four thread, 4GB RAM, 4 Intel(R) HD Graphics 3000, and NVIDIA GeForce GT 520MX 1024 MB Graphics Processor having 48 CUDA cores (Compute Unified Device Architecture). A sum of 12 CUDA cores has used to a maximum speedup of the image processing task by three times that of CPUs. For capturing footprint images, Canon 5400 digital scanner and EPSON Stylus CS5500 Scanner has utilized as a sensory module.

B. OPERATING SYSTEM AND TOOLS

The operating system for this system is Microsoft Windows 10 (10.0) Professional 64-bit (Build 2004). This experimentation utilizes ImageJ tool for raw image data capture, BigML for analysis of footprint morphology based on statistical parameters, IBM Watson Analytics is used for statistical pattern analysis, MATLAB 2016b (64 bit) is used for evaluation and implementation of algorithms.

C. DATASET

Currently, only two datasets are available for experimentation on the human biometric footprint images. Nagwanshi and Dubey [44] uploaded the first one in IEEE Dataport open access repository. The author has captured the left footprint

TABLE 1. Comparison of Accuracy of state-of-the-art alternatives.

Authors	Methodology	Observation	Accuracy
1. Nakajima <i>et al.</i> [6]	Euclidean distance	User should make stand up posture every time; recognition rate is insufficient for practical uses; only 10 subjects.	85%
2. Jung <i>et al.</i> [7]–[9]	Unconstrained dynamic footprint, Hidden Markov Model blended Levenberg-Marquart learning.	Highly correlated data; only 11 subjects.	64% to 80%.
3. Yun <i>et al.</i> [11]	Neural Network based Biometric User Identification with Dynamic Footprint.	10 subjects while walking over the <i>Ubi-FloorII</i> ; 10 subjects.	92% to 96 %
4. Uhl and Wild [4], [12], [13]	Eigenfeet, Ballprint and Foot geometry biometrics	Only 16 subjects.	97%
5. Qian <i>et al.</i> [29], [30]	3D trajectories of the center of foot pressures atop a footstep pressure sensing floor	Only 11 subjects in different walking styles	92.3%
6. Wang <i>et al.</i> [20]	Wavelet and fuzzy neural networks; four different shapes (triangle, ellipse, circular and irregular)	80 samples extracts 320 toe images for different shapes	92.8%
7. Takeda <i>et al.</i> [16]	Fuzzy load distribution sensor.	Employed 30 subjects	86%
8. Ye <i>et al.</i> [19]	ANN; K-out-of-n;	11 volunteers (10 samples/volunteer)	71.4% and 88.0%.
9. Takeda <i>et al.</i> [17], [18]	One Step Foot Pressure Distribution	10 subjects ; AIS has evaluated by the five-fold cross validation technique	96%
10. Kumar <i>et al.</i> [21]	Modified sequential haar energy transform technique	Euclidean distance compares MHE feature	92.37%
11. Lu and Tan [31]	Uncorrelated discriminant simplex analysis (UDSA)	Sequences of 124 subjects obtained from two distinct views	50% to 90%
12. Pataky <i>et al.</i> [23]	Foot pressure; Orthotics examination classification method	1040 dynamic foot pressure patterns; 10 volunteers (104 samples per subject)	99.6 % Classification Rate.
13. Jia <i>et al.</i> [32]	Online footprint based system for newborn and infant	1938 images from 101 newborns	96%
14. Kumar <i>et al.</i> [27], [33]–[35]	Manifold feature extraction; PCA with SVM	Feature has extracted based on Gabor filter and DWT	90.35%.
15. Khokher <i>et al.</i> [36]	PCA and ICA	21 subjects	95%
16. Hashem and Ghali [28]	ANN composed of a 16-node input layer, 11-node hidden layer, and 6-node output	Only 40 subjects; heavy computation loads.	92%
17. Kushwaha <i>et al.</i> [37], [38]	Footprint Minutiae and texture feature	160 Classes; 80 subjects; 5 images per subject	86 to 97%
18. Gupta <i>et al.</i> [37], [38]	Distance metric for touch less footprint	60 subjects; 5 images per subject; heavy computation loads.	84 to 97%
19. FKNN	Fine KNN	220 subjects; 6 images per subject;	91.11%
20. FSVM	Fine Gaussian SVM (Fuzzy Kernel)	220 subjects; 6 images per subject;	87.77%
21. Proposed FESD	Fuzzy Ensemble Subspace Discriminant	220 subjects; 6 images per subject;	98.89%

from 220 volunteers at the various hue and saturation levels to produce 6 different images at different time periods. Kumar [45] uploaded the second to the GitHub repository in the year 2019. For 21 persons, Two to five images per subject had captured using a flatbed scanner, and further, he has extended his dataset for 32 individuals as dactyloscopic images.

This research work has begun with pre-processing phase. Original footprints have captured using a conventional EPSON Stylus CS5500 scanner (see setup shown in Fig. 1) from 220 volunteers of Rungta College of Engineering and Technology Bhilai, India. These footprints have normalized for further experimentation. Twenty-one statistical feature has extracted for $220 \times 6 = 1320$ multi-spectral footprint images. The obtained dataset has published for evaluation purpose. The dataset has tested for applicability in further experimentation. The dataset has created for 880 footprint images; later it has created for 1320 footprint images from 220 volunteers. The first impression of images are shown in Table 2.

III. EXPERIMENTAL SETUP

Fig. 1 shows the experimental setup for footprint acquisition using EPSON Stylus CS5500 flatbed scanner. The subject needs to put his/her foot over the scanning plane. The scanner has the flexibility to scan in multiple-band and with multiple resolutions. The final outcome of the captured images has been published at IEEE Dataport [44].

A. EXTRACTED FEATURES

The segmented image has processed through ImageJ application to obtained the features. These features include area, mean gray value, standard deviation, modal gray value, minimum gray value, maximum gray value, centroid, the center of mass, perimeter, bounding rectangle, fit an ellipse, feret, circularity, roundness, median, mean, kurtosis and area fraction [46]–[48]. Let us describe each feature in brief. The dataset has been created for segmented images using the Algorithm 1 and analysed using Algorithm 2 as described in [49]. Let us describe each features in brief.

TABLE 2. Footprint sample of all 220 persons.

001	002	003	004	005	006	007	008	009	010	011	012	013	014	015	016	017	018	019	020
021	022	023	024	025	026	027	028	029	030	031	032	033	034	035	036	037	038	039	040
041	042	043	044	045	046	047	048	049	050	051	052	053	054	055	056	057	058	059	060
061	062	063	064	065	066	067	068	069	070	071	072	073	074	075	076	077	078	079	080
081	082	083	084	085	086	087	088	089	090	091	092	093	094	095	096	097	098	099	100
101	102	103	104	105	106	107	108	109	110	111	112	113	114	115	116	117	118	119	120
121	122	123	124	125	126	127	128	129	130	131	132	133	134	135	136	137	138	139	140
141	142	143	144	145	146	147	148	149	150	151	152	153	154	155	156	157	158	159	160
161	162	163	164	165	166	167	168	169	170	171	172	173	174	175	176	177	178	179	180
181	182	183	184	185	186	187	188	189	190	191	192	193	194	195	196	197	198	199	200
201	202	203	204	205	206	207	208	209	210	211	212	213	214	215	216	217	218	219	220

- **Area**– Footprint Area covered by a rectangle in square pixels. This is not convex hull area of a footprint; therefore area is coming same for all the footprint images. Fig. 2, shows the footprint surrounded by a red rectangle with height 666 pixels and width 256 pixels. In this case it is $256 \times 666 = 170496$ for all the normalized image.
- **Mean Gray Value**– is the sum of the gray values (here all 1's added together) in the selection divided by the area. It estimated average gray value for the selected footprint. See Fig. 5 which highlights both convex hull area supported by pixel value 1, and the complementary dark area. This feature received unique values for all the footprints.
- **Standard Deviation** – Standard deviation of total convex hull area used to generate the mean gray value above (See Fig. 5).
- **Modal Gray Value** – The highest frequency of pixel value in the bounding box shown in Fig. 5, represents the modal gray value. Because there are only 0 and 1 will the pixel value for any point, the result may come concerning 0 or 1. The modal gray value for all the images comes at level 1.
- **Min & Max Gray Level** - Always yields 0 or 1 because of a binary image (See Fig. 5).
- **Centroid (X, Y)** – The center point of the bounded box shown in Fig. 2 represents centroid. For this research work the centroid (X,Y) is always reported at $256/2=128$ and $666/2 =333$ ie [128,333].
- **Center of Mass (XM, YM)** – is the center of gravity of the convex hull of the foot. These coordinates are in the first order spatial moments. In Fig. 5, the cross circle mark represents the center of mass of the footprint.



FIGURE 1. Experimental setup for footprint acquisition using EPSON Stylus CS5500 flatbed scanner.

Algorithm 1 Random Subspace Algorithm

Require: input test sets \vec{x} ,
Require: with d features /columns /dimensions
 { m be the number of features to sample space for each learner. }
 { n be the number of learners in ensemble. }
 1: $i \leftarrow n$
 2: **repeat**
 3: Choose unique random set of m predictors from the d features / dimension.
 4: $train(weaklearner_i, m, y)_{i=1}^n$
 5: $i \leftarrow i - 1$
 6: **until** there are n weak learners.
 7: $predict(HighestAvgScore, weaklearner_i)_{i=1}^n$

- **Perimeter** – The total length of the outside boundary surrounds the footprint. Always same, i.e. from Fig. 2, it yields $(2 \times 256 + 2 \times 666) = 1844$ pixels for all normalized footprint images.
- **Bounding Rectangle (BX,BY,Width,Height)** – The smallest red colored rectangle enclosing the footprint in Fig. 2 represents the bounding rectangle. Here the value of bounding rectangle parameters represented as $[BX,BY,Width,Height] = [0,0,256,666]$ for all the footprint images in the dataset.
- **Fit Ellipse** – This is a combination of features which fits an ellipse to the selection [47], [48]. Fig. 3, describes fitting an ellipse for the footprint image shown in blue color. It is not necessary that it appears inside the bounding rectangle as shown in Fig. 3, it can cross the

Algorithm 2 Discriminant Analysis Model

Require: input test sets \vec{x} ,
Require: with d features /columns /dimensions { constructs weighted classifiers M is an $N - by - K$ class membership matrix }
 1: $M(n, k) \leftarrow \begin{cases} 1 & \text{if observation } n \text{ is from class } k \\ 0 & \text{otherwise} \end{cases}$
 { Estimate the class mean for unweighted data. }
 2: $\mu_k \leftarrow \frac{\sum_{n=1}^N M(n, k)x_n}{\sum_{n=1}^N M(n, k)}$
 { Estimate the class mean for positive weighted data with weight w_n }
 3: $\mu_k \leftarrow \frac{\sum_{n=1}^N M(n, k)w_n x_n}{\sum_{n=1}^N M(n, k)w_n}$
 { Find the weighted sum ω_k for classes k }
 4: $\omega_k \leftarrow \sum_{n=1}^N M(n, k)w_n$ { Find the squared weighted sum ω_k^2 for classes k }
 5: $\omega_k^2 \leftarrow \sum_{n=1}^N M(n, k)w_n^2$
 { The unbiased estimate of the pooled-in covariance matrix with weights sum to unity }
 6: $\Sigma \leftarrow \frac{\sum_{n=1}^N \sum_{k=1}^K M(n, k)w_n(x_n - \mu_k)(x_n - \mu_k)^T}{1 - \sum_{k=1}^K \frac{\omega_k^2}{\omega_k}}$

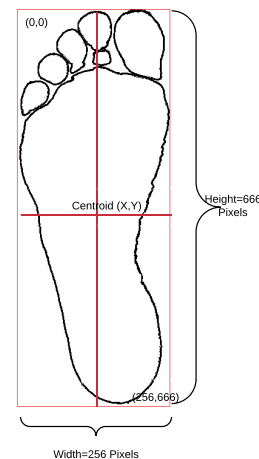


FIGURE 2. Various features of segmented footprint image: Footprint in a bounded box.

- boundary too depending upon the shape. The elliptical parameter includes a major axis, minor axis, and angle. The coordinates of the center of the ellipse displayed as X and Y . For all the normalized images the length of major axis comes 751.501 pixel, the minor axis comes 288.865 pixel, angle is 90° , and the crossing point of major and minor axis is the centroid (X, Y) .
- **Circularity** – Circularity is a shape descriptor calculated by Eq. 1. For normalized footprint the shape descriptor circularity is obtained as 0.63.

$$circularity = \frac{4 \times \pi \times area}{perimeter^2}$$

$$circularity = \frac{4 \times \pi \times 256 \times 666}{[2 \times (256 + 666)]^2} = 0.63 \quad (1)$$

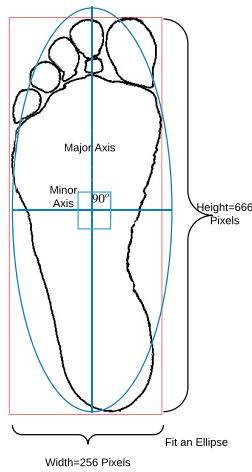


FIGURE 3. Various features of segmented footprint image: Footprint fits an ellipse.

- **Aspect Ratio** – The ratio between height and width is known as aspect ratio as shown in Eq. 2.

$$AR = \frac{height}{width}$$

$$AR = \frac{666}{256} = 2.602 \quad (2)$$

- **Roundness** – Roundness is another shape descriptor computed by Eq. 3 [48].

$$round = \frac{4 \times area}{\pi \times height^2}$$

$$round = \frac{4 \times 256 \times 666}{\pi \times 666^2} = 0.384 \quad (3)$$

- **Solidity** – The ratio between area and convex area for a segmented footprint image gives solidity of shape. It represents a value 1 which shows the shape is perfectly solid.
- **Feret’s Diameter** – Fig. 4 shows the longest distance from toe to heel of the foot, also known as maximum caliper [48].
- **FeretAngle** – It is the angle between the Feret’s diameter and a line parallel to the x-axis of the image as shown in Fig. 4. For all normalized footprint image it is coming 111.026° .
- **Minimum Feret** – For a normalized footprint the minimum caliper diameter is coming 256 pixel.
- **Integrated Density** – In Fig. 5, the integrated density is calculated by the product of Area and Mean Gray Value; and the raw integrated density is the sum of the values of the pixels in the image or selection exhibits the same result for the footprint images.
- **Median** – The median value of the pixels in the footprint image or selection as shown in Fig. 5. For a binary image the value is always 1.
- **Skewness** – Skewness is the measurement of the symmetry represented by the third order moment about the

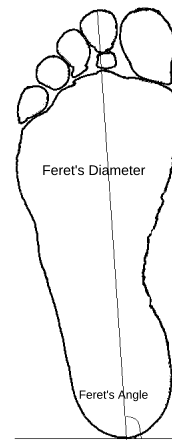


FIGURE 4. Various features of segmented footprint image: Measurements of feret.

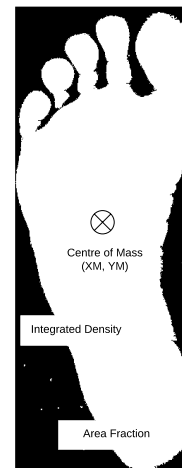


FIGURE 5. Various features of segmented footprint image: Measurement of center of mass, Integrated density, and area fraction.

mean. The coefficient of skewness is zero for symmetric distribution, less than zero for asymmetric distribution to the left where tail extends left of the center of mass, and greater than zero for asymmetric distribution to the right where tail extends right of the center of mass.

- **Kurtosis** – Kurtosis is the fourth order moment about the mean, and it shows flatness in x and y. The coefficient of kurtosis is zero for Gaussian distribution, less than zero for distribution flatter than normal, greater than zero for distribution more peaked than normal, and a constant -1.2 for or multimodal distribution.
- **Area Fraction** – The percentage of pixels in the image or selection as shown in Fig. 5. For non-thresholded images, the area fraction is represented by the percentage of non-zero pixels.

The feature selection is done on the basis of data analysis of features. The grayscale images represent unique values for most of the features, but when go multispectral it is

showing more diversified results for the same class hence binary images are best alternative to perform experimentation where high degree of uniqueness per class is required.

IV. METHODOLOGY

This section presents design of Fuzzy Inference System for footprint based system. This FIS has been applied into the algorithms presented in next sections. This section also explains FIS with the help of grid partitioning method and subspace clustering system. On the basis of examination of these features in [50], only eight principle features have been selected for the experimentation. These features include area, integrated density, centre of mass (XM , YM), skewness, kurtosis and standard deviation of segmented footprints.

A. FUZZY ENSEMBLE SUBSPACE DISCRIMINANT BASED FOOTPRINT MATCHER

The ensemble is modern approach combines the outcome of multiple conventional methods to get faster and better output. The training set consists of input features called predictors, and the out classes are known as the response. There are several aggregation methods for ensemble approach. Because footprint based method involves in identifying multiple classes, it can use AdaBoost, LPBoost, TotalBoost, RUSBoost, Subspace, and Bag as aggregation method. There are three weak learners *viz.* discriminant, KNN, and tree. The tree is not recommended with subspace aggregator, while discriminant and KNN is recommended with subspace. Fuzzy logic can be applied to weak learners. According to [51], the subspace method generates multiple independent parallel subspace makes faster learning without hill climbing and local optima. For discriminant analysis it is required to choose the optimum value of K in FKNN. Create the ensemble subsequently for 2-nearest neighbor classification with diversified set of dimensions and finally, this algorithm attempts in finding the optimum number of learners for best result. Initially, the Algo. 1, starts with loading the footprint dataset for eight predictors and one response. In the next step, it creates subset of d , into m for n learners. For each weak learner i , it is trained against y , with m number of features. This training runs until no weak learners available to train. Finally, the prediction is completed using highest average scores among these weak learners. Algorithm 2, presents a straightforward way to create discriminant analysis model.

Suppose A is a manual table of footprint for *a-priori* split of n data items into k different classes. This is a boolean table represents binary crisp membership data to the one of the classes k . To make decision more realistic let convert A into fuzzy set. For a given dataset $X = \{x_1, x_2, \dots, x_n \subset R^s$, the optimal fuzzy set \tilde{A} , with associated prototype $L \subset R^s$, and an *a-priori* constant $\eta > 0$, the fuzzy objective function is given as Eq. 4.

$$\text{minimize } \phi(\tilde{A}, L) = \sum_{j=1}^n \tilde{A}(x_j)^m \|x_j - L\|^2$$

$$+ \sum_{j=1}^n (1 - \tilde{A}(x_j))^m \left(\frac{\eta}{1 - \eta} \right)^{m-1} \quad (4)$$

subject to $m > 0$ is the fuzzy membership degree. The value of $\tilde{A}(x_j)$, can be obtained from Eq. 5.

$$\tilde{A}(x_j) = \frac{\eta/(1 - \eta)}{\eta/(1 - \eta) + \left(\frac{\|x_j - L\|}{\max \|x_j - L\|} \right)^{2/(m-1)}} \quad (5)$$

The fuzzy discriminant analysis method presented here is a multiclass method by design, as no restriction with respect to the number of classes is introduced. This is a parameter to be set by the human experts as they establish the a-priori classes split. The FESD algorithm generates following set of rules. Following rules have been written in verbatim mode. Graphical mode representation have been listed in Fig. 30 in page 26657.

V. RESULTS

A set of $220 \times 6 = 1320$ multi-spectral foot images have taken into account. It is challenging to represent characteristics of all 1320 images. Therefore, a sum of 15 classes have taken to reflect the precise results [52]. All the algorithms have trained with original multi-spectral dataset and test using median and average value of each class. Table 3, explores the dataset for six samples and its median and average values (total 8 samples). This is helpful in testing the algorithms. Each algorithm has trained for known six samples per class and test with the average and median values. In this case training testing pair is having 75:25 ratio or 6:2 ratio. Fig. 7 gives the comparison of testing and training error. Fig 7, represents the comparison of training error with 75% samples, on the other hand Fig 6, represents the testing error with 25% samples against the training samples.

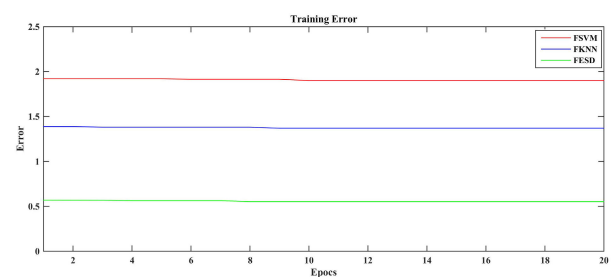


FIGURE 6. Training performance of FSVM, FKNN and FESD.






A. CONFUSION MATRIX

A confusion matrix is an important table used here to describe the performance of a footprint based matching algorithm on a set of test data for which the true values are known.

B. NUMBER OF OBSERVATIONS

The confusion matrix based on number of observations per class are shown in Fig. 8. For number of samples $N + P$ and false matches TP , the accuracy can be calculated by

TABLE 3. Sample dataset of five persons with median and average.

Class	Data									
	Mean	StdDev	XM	YM	IntDen	Skew	Kurt	%Area	Class	
	0.642	0.479	140.525	316.150	109410.000	-0.591	-1.651	64.172	1	
	0.656	0.475	140.669	314.710	111810.000	-0.656	-1.570	65.579	2	
	0.638	0.481	140.518	316.781	108820.000	-0.575	-1.669	63.826	3	
	0.642	0.480	140.532	316.142	109388.000	-0.591	-1.651	64.159	4	
	0.635	0.481	140.454	317.000	108259.000	-0.561	-1.686	63.497	5	
	0.638	0.481	140.482	316.540	108765.000	-0.574	-1.671	63.793	6	
	0.640	0.481	140.522	316.345	109104.000	-0.583	-1.660	63.993	Median	
	0.642	0.480	140.530	316.221	109408.667	-0.591	-1.650	64.171	Average	
		0.640	0.480	136.012	318.713	109033.000	-0.581	-1.662	63.950	1
		0.655	0.475	135.813	316.766	111631.000	-0.651	-1.576	65.474	2
0.637		0.481	136.012	319.144	108591.000	-0.569	-1.676	63.691	3	
0.640		0.480	136.012	318.713	109033.000	-0.581	-1.662	63.950	4	
0.635		0.481	136.031	319.269	108267.000	-0.561	-1.685	63.501	5	
0.637		0.481	136.023	319.060	108672.000	-0.572	-1.673	63.739	6	
0.639		0.481	136.012	318.887	108852.500	-0.577	-1.668	63.845	Median	
0.641		0.480	135.984	318.611	109204.500	-0.586	-1.656	64.051	Average	
		0.588	0.492	126.978	313.642	100265.000	-0.358	-1.872	58.808	1
		0.607	0.488	127.168	312.039	103447.000	-0.437	-1.809	60.674	2
	0.584	0.493	126.933	314.213	99608.000	-0.342	-1.883	58.422	3	
	0.588	0.492	126.978	313.642	100265.000	-0.358	-1.872	58.808	4	
	0.582	0.493	126.983	314.622	99164.000	-0.331	-1.890	58.162	5	
	0.585	0.493	126.949	314.095	99818.000	-0.347	-1.880	58.546	6	
	0.587	0.493	126.978	313.869	100041.500	-0.353	-1.876	58.677	Median	
	0.589	0.492	126.998	313.709	100427.833	-0.362	-1.868	58.903	Average	
		0.606	0.489	128.118	316.617	103378.000	-0.435	-1.811	60.634	1
		0.625	0.484	128.361	315.074	106581.000	-0.517	-1.733	62.512	2
0.604		0.489	128.062	317.013	102929.000	-0.424	-1.820	60.370	3	
0.606		0.489	128.118	316.617	103378.000	-0.435	-1.811	60.634	4	
0.602		0.490	128.051	317.159	102565.000	-0.415	-1.828	60.157	5	
0.604		0.489	128.069	316.967	102987.000	-0.425	-1.819	60.404	6	
0.605		0.489	128.094	316.792	103182.500	-0.430	-1.815	60.519	Median	
0.608		0.488	128.130	316.575	103636.333	-0.442	-1.804	60.785	Average	
		0.667	0.471	140.203	316.878	113740.000	-0.709	-1.497	66.711	1
		0.661	0.473	140.269	317.514	112739.000	-0.681	-1.536	66.124	2
	0.664	0.472	140.218	317.239	113256.000	-0.696	-1.516	66.427	3	
	0.667	0.471	140.206	316.874	113758.000	-0.710	-1.496	66.722	4	
	0.663	0.473	140.294	317.297	112976.000	-0.688	-1.527	66.263	5	
	0.665	0.472	140.228	317.250	113391.000	-0.699	-1.511	66.507	6	
	0.665	0.472	140.223	317.245	113323.500	-0.698	-1.514	66.467	Median	
	0.665	0.472	140.236	317.175	113310.000	-0.697	-1.514	66.459	Average	

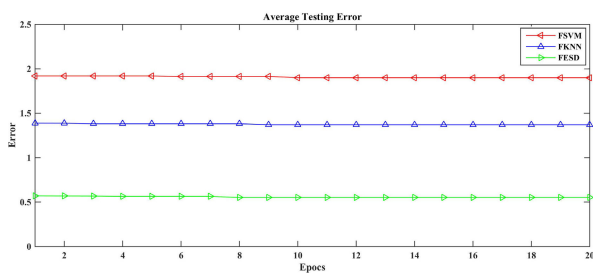


FIGURE 7. Average testing performance of FSVM, FKNN and FESD.

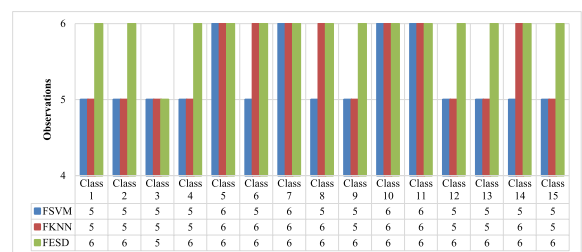


FIGURE 8. Number of true observations obtained from confusion matrix.

$ACC = (TP + TN)/(P + N) = 1 - EER$. Fine Gaussian SVM approach has shown in Fig. 9, depicts total 11 number of false matches out of 90 combinations, hence, it shows accuracy of 87.77%. Confusion matrix of Fine KNN approach is shown in Fig 10, exhibits 8 number of false matches out of 90 combinations, therefore, it gives accuracy of 91.11%. Confusion matrix of Fuzzy Ensemble Subspace Discriminant approach as shown in Fig. 11 exhibits accuracy of 98.89%

with only one false match out of 90. Fig. 8, summarizes the number of true matches for different approaches.

C. TRUE POSITIVE RATE/FALSE NEGATIVE RATE

This observation is based on true classes to predictive classes. Fig. 12 reveals the confusion matrix for true positive rate and false negative rate. Last green column gives the values of true positive rate, and the column with peach color gives the value of false negative rates. It also gives the comparison

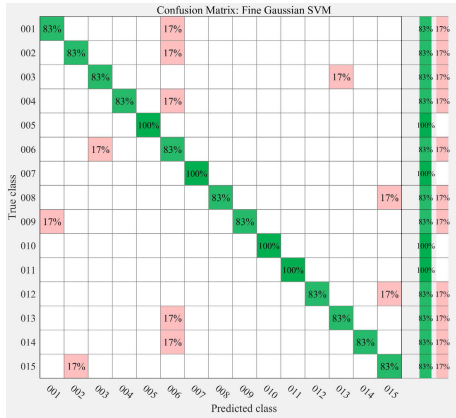


FIGURE 9. Confusion Matrix : Based on number of observations per class Fine Gaussian SVM approach.

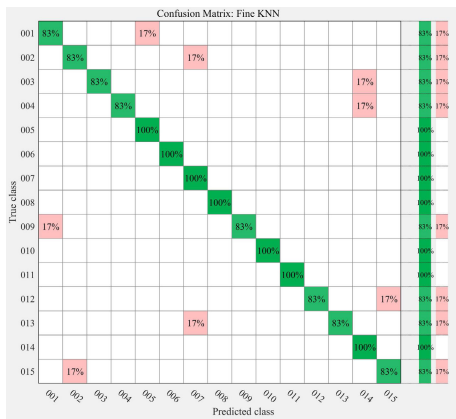


FIGURE 10. Confusion Matrix : Based on number of observations per class Fine KNN.

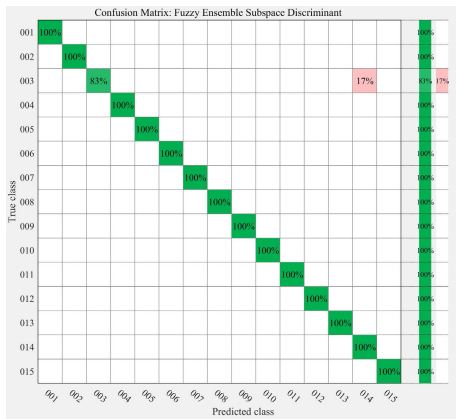


FIGURE 11. Confusion Matrix : Based on number of observations per class Fuzzy Ensemble Subspace Discriminant.

of TPR for FSVM, FKNN, and FESD approaches. Table 4 gives the comparison of FNR for FSVM, FKNN, and FESD approaches. Table 4 gives the Comparison of average TPR and average FNR. The average TPR for Fine Gaussian SVM approach has observed 0.8757. For Fine KNN, the observed

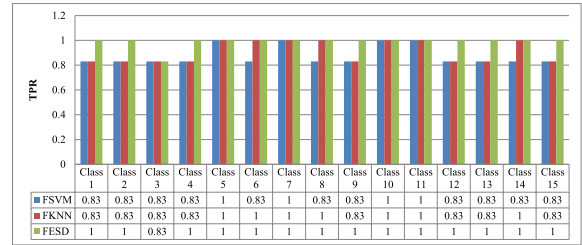


FIGURE 12. Comparison of True positive rate.

TABLE 4. Comparison of average TPR and average FNR.

Approach	Average TPR	Average FNR
FSVM	0.8757	0.1246
FKNN	0.9093	0.0906
FESD	0.9886	0.0113

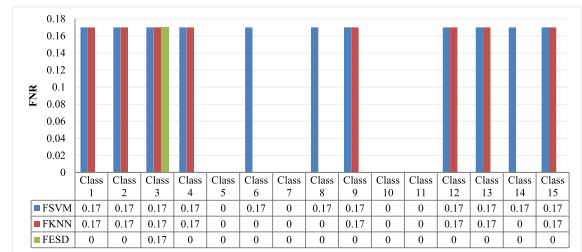


FIGURE 13. Calculation of False negative rates.

TABLE 5. Comparison of average PPV and average FDR (in %).

Approach	PPV	FDR
FSVM	90.20%	9.80%
FKNN	92.33%	7.60%
FESD	99.06%	0.93%

average TPR value is at 0.9093. And, finally an average TPR of 0.9886 has observed for Fuzzy Ensemble Subspace Discriminant approach. From Fig. 13 the average FNR for Fine Gaussian SVM approach has observed 0.1246, or Fine KNN, the observed average TPR value is at 0.0906, and, finally an average FNR of 0.0113 has observed for Fuzzy Ensemble Subspace Discriminant approach.

D. POSITIVE PREDICTIVE VALUES/FALSE DISCOVERY RATES

Based on confusion matrix for Positive Predictive Values and False Discovery Rates. The lower row with green color gives the values for Positive Predictive Values for each classes, while the lower row in peach, red and white color indicates the False Discovery Rates. Class 6 gives PPV and FDR of 0.5 each using FSVM approach. This is not good result for a good matcher. Here features of true classed 1, 2, 4, 13, and 14 matched 0.010 each to predicted class 6. Another true classes 8, and 12 also matched with the features of class

TABLE 6. Class wise summary of ROC for FSVM, FKNN, FESD approach.

Method	ROC	1	2	3	4	5	6	7	8	9	10	11	12	13	14	15
FSVM	TPR	0.83	0.83	0.83	0.83	1	0.83	1	0.83	0.83	1	1	0.83	0.83	0.83	0.83
FSVM	FPR	0.01	0.01	0.01	0	0	0.06	0	0	0	0	0	0	0.01	0	0.02
FSVM	AUC	0.89	0.86	0.88	0.87	1	0.87	1	1	0.87	1	1	0.87	0.89	0.87	0.86
FKNN	TPR	0.83	0.83	0.83	0.83	1	1	1	1	0.83	1	1	0.83	0.83	1	0.83
FKNN	FPR	0.01	0.01	0	0	0.01	0	0.02	0	0	0	0	0	0	0.02	0.01
FKNN	AUC	0.91	0.91	0.92	0.92	0.99	1	0.99	1	0.92	1	1	0.92	0.92	0.99	0.91
FESD	TPR	1	1	0.83	1	1	1	1	1	1	1	1	1	1	1	1
FESD	FPR	0	0	0	0	0	0	0	0	0	0	0	0	0.01	0	0
FESD	AUC	1	1	1	1	1	1	1	1	1	1	1	1	1	1	1

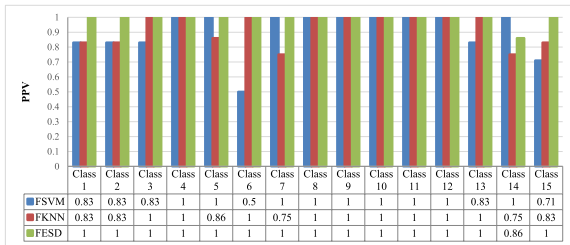


FIGURE 14. Comparison of positive predictive values.

TABLE 7. Average receiver operating characteristics for FSVM, FKNN, FESD approach.

ROC	FPR	TPR	AUC
FSVM	0.01	0.88	0.92
FKNN	0.01	0.91	0.95
Foot Geometry Biometrics	0.01	0.92	0.94
UDSA	0.01	0.93	0.95
Manifold Feature Extraction	0.01	0.90	0.92
FESD	0.00	0.99	1.00

15 leads to FDR of 0.29. FSVM and FKNN, both exhibits FDR for 6 classes. While, FESD shows FDR for only one class. Fig. 12, gives the comparison of TPR for FSVM, FKNN, and FESD approaches.

Table 5 gives the Comparison of average PPV and average FDR. The average PPV for Fine Gaussian SVM approach has observed 90.20%. For Fine KNN, the observed average PPV value is at 92.33%. And, finally an average PPV of 99.06% has observed for Fuzzy Ensemble Subspace Discriminant approach. Fig. 15, gives the comparison of FDR for three approaches. The average FDR for Fine Gaussian SVM approach has observed 9.8%. For Fine KNN, the observed average TPR value is at 7.6%. And, finally an average FNR of 0.93% has observed for Fuzzy Ensemble Subspace Discriminant approach.

E. ROC:RECEIVER OPERATING CHARACTERISTIC

ROC curves obtained in this experimentation gives the trade-off between footprint matching sensitivity (TPR) and footprint matching Fall-Out(FPR) or specificity (TNR) as $FPR = 1 - TNR$ for all possible cut-off for a test or its

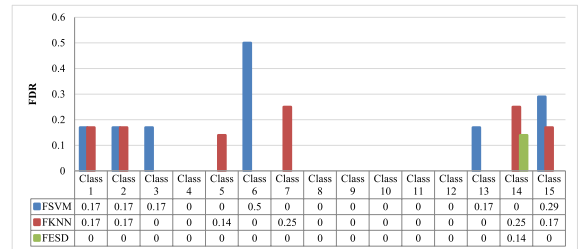


FIGURE 15. Comparison of false discovery rates.

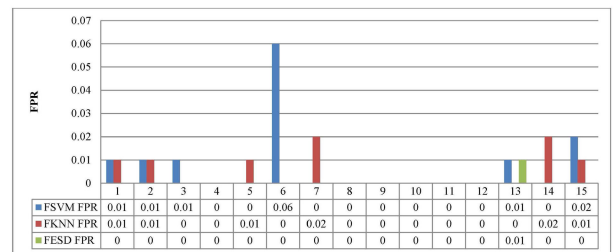


FIGURE 16. Comparison of False positive rates.

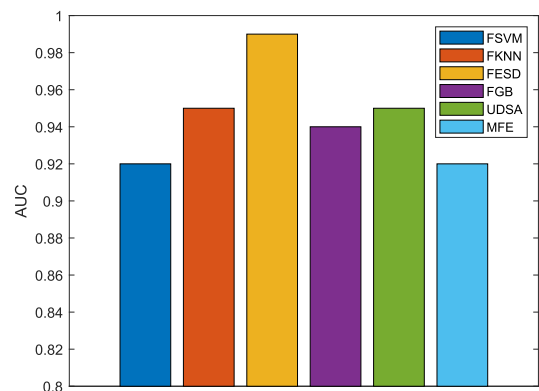


FIGURE 17. Comparison of Area under the ROC curve.

combination. Also, the area under the ROC curve (AUC) presents an idea about the advantage of employing the test(s), which is a measure of the usefulness of an experiment. The best cut-off has the highest true positive rate together with the lowest false positive rate leads to a greater area. The TPR values can be obtained from Fig. 12, and the values of FPR is

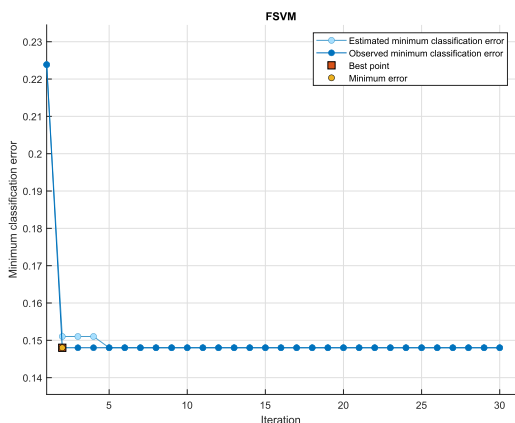


FIGURE 18. Classification Error Plot: FSVM.

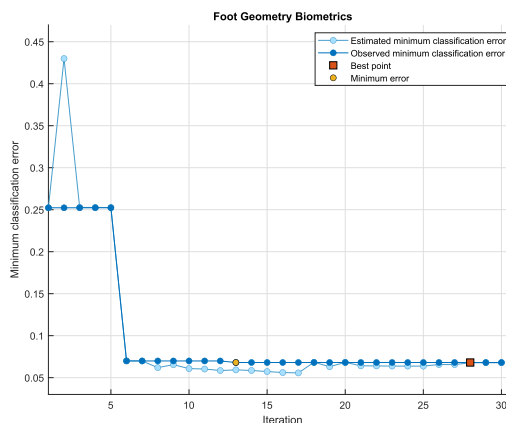


FIGURE 21. Classification Error Plot: Eigenfeet, Ballprint and Foot geometry biometrics. [4], [12], [13]

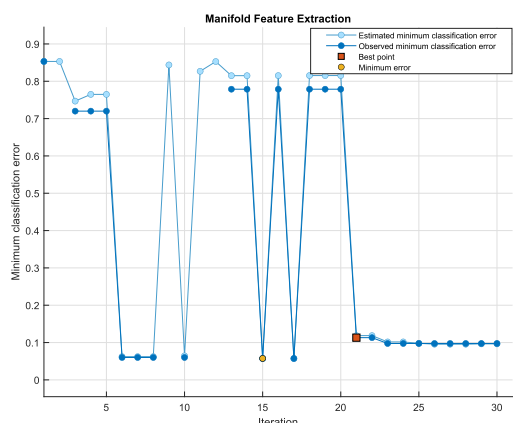


FIGURE 19. Classification Error Plot: Manifold feature extraction (PCA with SVM) [27], [33]–[35].

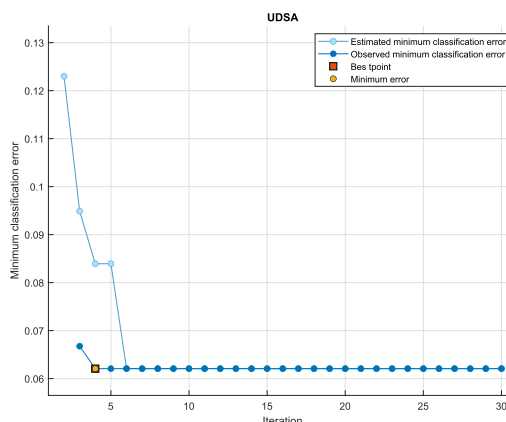


FIGURE 22. Classification Error Plot: Uncorrelated discriminant simplex analysis (UDSA). [31]

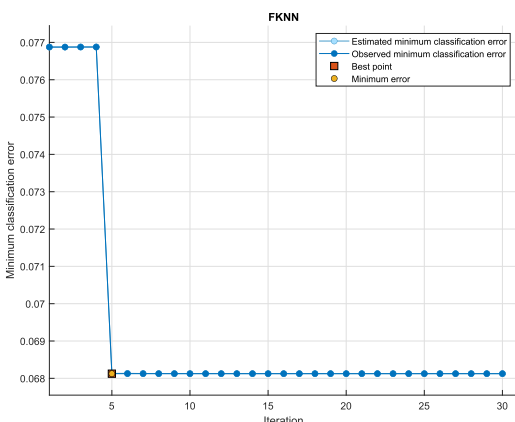


FIGURE 20. Classification Error Plot: FKNN).

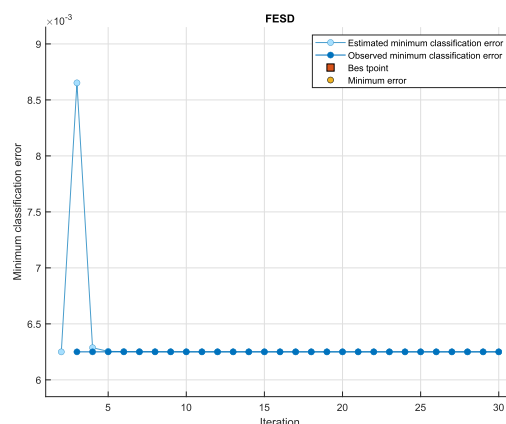


FIGURE 23. Classification Error Plot:FESD.

listed in Fig. 16. Table 6 gives class wise summary of ROC for FSVM, FKNN, FESD approach. Average receiver operating characteristics for FSVM, FKNN, FESD approach for above listed figures and table has concluded in Table 7. It shows (0.01,0.88) cut-off with 0.92 AUC for FSVM, (0.01,0.91) cut-off with 0.95 AUC for FKNN, and (0.00,0.99) cut-off with 1.00 AUC for FESD approach.

F. COMPARATIVE ANALYSIS OF THE STATE-OF-THE-ART METHODS

In the previous subsection, the study discussed three methodologies implemented for footprint-based identification. This section compares state-of-the-art-methods implemented with the dataset created for this study [44]. The study of footprint

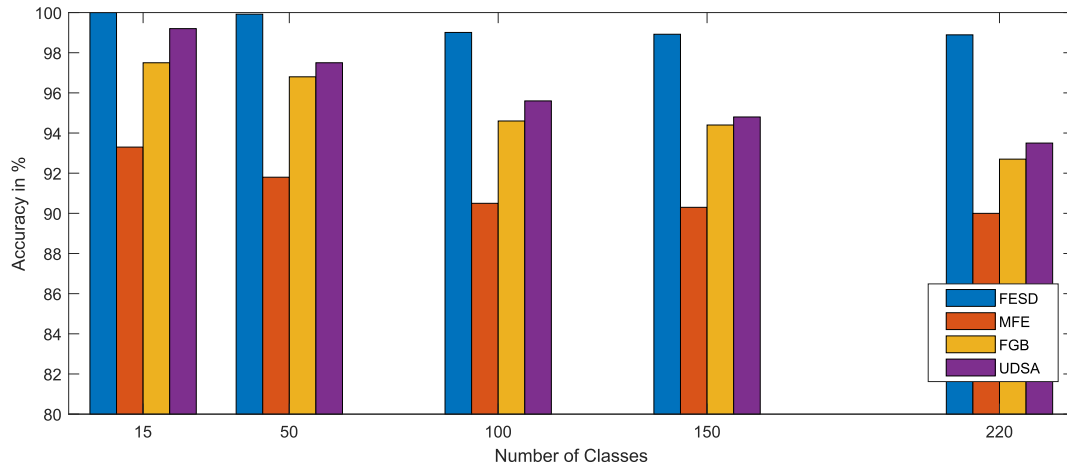


FIGURE 24. Comparison of Accuracy.

presented in this article utilizes three techniques: Eigenfeet, Ballprint, and Foot geometry biometrics developed by Uhl and Wild [4], [12], [13], Manifold feature extraction using PCA with SVM produced by Kumar et al. [27], [33]–[35] and Uncorrelated discriminant simplex analysis (UDSA) given by Lu and Tan [31].

Table 7 and Fig. 17 gives a comparative analysis of AUC parameters. The AUC of FSVM is 0.92, FKNN recorded at 0.95, FESD at 0.99, Foot Geometry Biometrics at 0.94, UDSA at 0.95, and Manifold Feature Extraction at 0.92 level. The obtained parameters justifies the implemented method.

Fig. 24 gives the comparative plot of accuracy obtained for the proposed method with existing three methods as discussed. For around 400 samples or 50 classes all the methods show better results. As we increase the number of samples the accuracy of different method gradually decreases. FESD exhibits almost stable behavior beyond 50 classes at accuracy reading of 98.89%.

Fig. 18 to Fig. 23 represents the classification error plots for first 30 iterations. The Manifold feature extraction using PCA with SVM shown in Fig. 19 exhibits unstable characteristics upto 20 iterations. The classification error can be calculated as a fraction of number of miss-classifications to total number of samples [53]. Fig. 25 gives the comparative plot of classification error with respect to the increase in number of classes. Among all methods FESD reported lowest classification error of 0.004545455 level.

Fig. 26 gives a logarithmic comparison of training time to the increased number of samples. The FESD shows the minimum training time while the algorithm based on PCA and SVM requires more time than all other listed approaches (almost exponential). Table 8 presents a detailed analysis of training to the number of classes introduced for the time taken by different approaches to produce the result.

VI. DISCUSSIONS

Several methods have been studied for evaluation of performance. Nakajima et al [6] achieved 85% recognition rate with

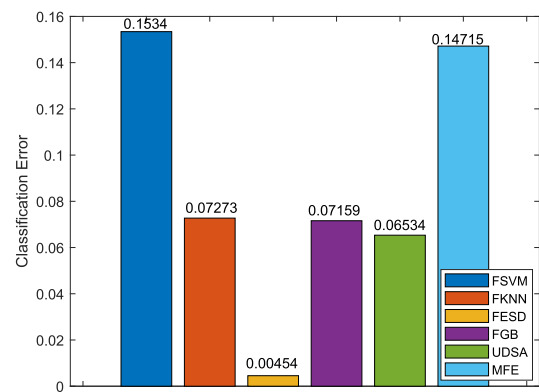


FIGURE 25. Comparison of Classification Error.

TABLE 8. Comparison of Training Time.

Algo. Clas-ses	FSVM Proposed	FKNN	FESD	FGB [12] [4], [13]	UDSA [31]	MFE [27], [33] [34], [35]
15	31.37	32.37	8.251	38.32	46.39	216.86
50	68.15	1.16	4.88	68.91	68.78	222.12
100	188.62	1.52	7.59	40.05	68.72	334.56
150	812.20	1.95	11.97	31.97	43.26	729.29
220	1893.00	2.72	18.51	47.53	45.44	884.61

only 11 subjects, [4], [12], [13] claims the highest recognition rate of 97% with 16 subjects, while with 40 subjects [28] claims 92% of the recognition rate. This section summarize the result of data testing cross examined by different approaches.

- Section V on page 26647, gives the positive and negative data. The FSVM and FKNN give a large number of negative data for all eight features ranges from 7 to 11 outliers; while, the FESD approach provide a constant set of the outlier, which is only 2. Because centroids XM and YM are based on pixel position, the plot between Mean vs. XM, and Mean vs. YM exhibits a high

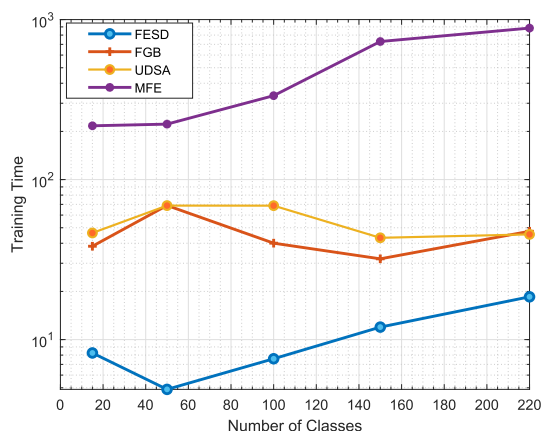


FIGURE 26. Comparison of Training Time.

degree of scattered characteristics. All the graphs show a linear characteristic proves that the statistical features are unique and identifiable from each other.

- Section V on also give the training and testing performance. The actual samples are six, median and average of each features crated 2 more rows of dataset. The algorithm has trained using these 75% samples and tested against 25% samples. Training and testing performance overlaps on each other. FSVM algorithm exhibits a training error of 1.9008 with the same amount of average testing error. FKNN algorithm shows a training error of 1.3693 with the same amount of average testing error. FESD algorithm exhibit a training error of 0.55193 with the same amount of average testing error. All three algorithms represents better characteristics, and the FESD algorithm performs best among all the three.
- Section V-A on page 26647, provides description of confusion matrix for various performance measurement parameters. Number of true observation has calculated for 15 classes. The FSVM exhibits 87.77% accuracy, FKNN represents 91.11% accuracy, and FESD represents 98.89% accuracy which is best among three.
- The TPR or TMR for FSVM and FKNN are observed at 0.8757 and 0.9093 respectively, it is good value but not suitable for matching problem; while the TPR for FESD is reported at 0.9886 near to unity exhibits best value for the matching problem. On contrary, the FNR or FNMR are obtained as 0.1246 for FSVM, 0.0906 for FKNN, and 0.013 (best value is zero) for FESD. The true match ratio and false non match ratio gives the matching performance. The FESD approach proves best matching performance.
- The PPV of 0.902, 0.9233, and 0.9906 has obtained for FSVM, FKNN, and FESD approach respectively. The FDR has observed rates 0.098 for FSVM, 0.076 for FKNN, and 0.0093 for FESD approach. The PPV approaches nearly unity for FESD and a zero for FESD proves its discoverability or predictability of true footprint patterns.

- The FPR or FMR for FSVM is recorded a value of 0.01, for FKNN it is 0.007, and for FESD it is 0. This performance proves the robustness of FESD indicating no false match.
- The ROC is a characteristic plot between FPR and TPR. A sum of 15 samples discussed here for the validity of performance. The best value for Area under curve is 1. AUC ranges from 0.86 for FSVM to 1 for FESD. The overall AUC for FSVM is 0.92. FKNN is.095 and for FESD it is 1. The higher value shows the usefulness of employment of experimentation.
- Subsection V-F gives a comparison of implemented state-of-the-art methods with proposed approaches using the same dataset. It shows the accuracy of the methods concerning the number of subjects. It also justifies the proposed FESD approach with an accuracy of 98.89% and the minimum training time requirement.

VII. CONCLUSION

The first objective of the research work was to relate the traditional biometric features to an innovative biometric human footprint. In this regard, a comprehensive literature survey work has already completed in [39]. Further testing the footprints for its uniqueness using the traditional minutiae-based method and it exhibited a positive result in a direction to carry forward the research work.

The next objective of the research work was to meet all aspects of existing biometric characteristics to a new biometric modality human footprint. Universality is every subject in the system holds some features and human footprints hold a high number of features like minutiae, toeprint, the area of footprint, centroid and so forth. The uniqueness of footprint features has confirmed by Data Testing, FSVM, FKNN, and FESD algorithms. The permanence of features has proved by checking some random footprints in a timely order. The measurability or collectability is the simplicity of attainment or capacity of the features that permit further processing and extraction of the appropriate feature sets. The measurability tradeoff has useful in the creation of footprint dataset. Performance is the measurement of accuracy, speed, and robustness of algorithm used; and this has also proved by experimentation of FSVM, FKNN, and FESD. Footprint biometrics also exhibit acceptability concerning the measurement of acceptance of the technology for the biometric feature captured and arbitrated. And, finally, it is impossible to create footprints with same features. Therefore, the **circumvention** which denotes the ease with which a footprint features might be counterfeit is not possible.

The next objective was to study the applicability of biometric footprint approach in industries, government and public domain, and this was carried out with the help of extensive literature survey presented and publications [39].

The next objective was to rectify the match rate to reach the required accuracy of 98%, False Match Rate of value 0.01 (FMR, the rate of falsely as genuine classified imposters), and False Non-Match Rate at 0.01 level(FNMR, the rate of falsely

as imposter classified genuine users) to a set of different matchers. For this purpose, three algorithms FSVM, FKNN, and FESD were evaluated with the created dataset. The results are as per this objective and discussed in section VI.

The next objective was to ascertain the employability of the footprint concerning temporal, and physical features. For this purpose, some footprint sample has taken time to time from identified volunteers. The footprint matching performance does not affect, and this proved employability of the footprint concerning temporal, and physical features.

Fig. 26 shows improving the speed of recognition with 220 subjects was another objective. With the help of parallel processing using GPUs, it has increased recognition speed as training time decreases compared to the alternative approaches.

The next objective was to implement the prototype schemes for footprint biometric to evaluate system properties, including accuracy and performance. For this purpose, three algorithms have designed based on the fuzzy logic approach which fulfills this objective.

The final objective of this work was to promote it to install in legal capacities to identify the person or impostor. This objective has fulfilled by the publication produced.

VIII. FUTURE DIRECTION OF PRESENT RESEARCH WORK

Earlier work was based entirely on physical characteristics of footprints. Present work is based on fuzzy logic based enhanced matching technique for footprint identification proves its objective. Every research work has some limitations. Current practice was limited to statistical features and fuzzy logic domain. Fuzzy logic has a significant restriction of speedy performance, which cannot be entirely overcome by GPUs and parallel computing alone. The work can be further extensible to newer algorithms base on machine learning and soft computing technique with the fusion of statistical plus physical characteristics of human footprints. Adding other modalities such as iris, signature, fingerprints, voice etc. with footprint can give a more robust solution. Beside methods and hardware, one can implement the footprint biometrics matcher with the help of Mathematica, LabView, Python and such other tools for better scalability of results.

**APPENDIX A
FUZZY LOGIC IN FOOTPRINT IMAGING**

Zadeh [54], [55] established the innovative mathematical framework of Fuzzy logic. A fuzzy set consists of different classes of objects with membership participation in terms of a membership function showing a grade range between zero and one (both inclusive). He has given a new meaning to the union, the intersection, the complement, etc. of classical set theory. There are two representations of fuzzy inference systems Mamdani-type [56] and Sugeno-type [57], which vary moderately in the way outputs are determined. The footprint feature set in terms of fuzzy logic can be expressed as Eq. 6

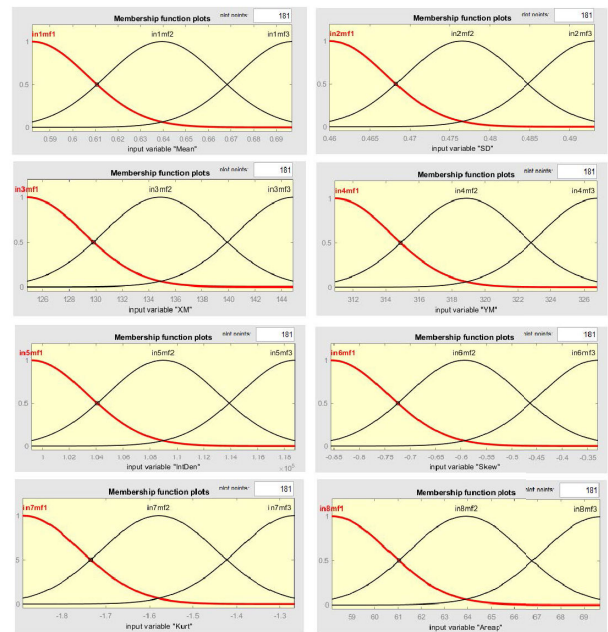


FIGURE 27. Input membership function plots.

[16], [18].

$$foot = \{Mean, StdDev, XM, YM, IntDen, Skew, Kurt, Area\} \quad (6)$$

A. FUZZIFICATION

The process begins with the fuzzification of the input set. Here the foot is represented as input set. But the foot itself consists of eight input sets. The universe of discourse for each input set is shown in Table 10. Initially, it is required to find the degree of membership belongs to each of the appropriate fuzzy sets through membership function. Present work utilizes following input membership function for all the three approaches. The output is a fuzzy degree of membership in the qualifying linguistic set (always the interval between 0 and 1). Fuzzification of the input amounts to either a table lookup or a function evaluation. It is a Gaussian type membership function. There are 8 inputs with one output. The Fig. 27 gives the input membership plot for all 8 features (Mean, StdDev, XM, YM, IntDen, Skew, Kurt, Area). Subsequently, it also shows some output membership functions.

1) INPUT MEMBERSHIP FUNCTIONS

```
[Input1]
Name='Mean'
Range=[0.582 0.697]
NumMFs=3
MF1='in1mf1': 'gaussmf',
[0.0244180017582805 0.582]
MF2='in1mf2': 'gaussmf',
[0.0244180017582805 0.6395]
MF3='in1mf3': 'gaussmf',
```

```
[0.0244180017582805 0.697]
```

```
[Input2]
Name='SD'
Range=[0.46 0.493]
NumMFs=3
MF1='in2mf1':'gaussmf',
[0.00700690485237615 0.46]
MF2='in2mf2':'gaussmf',
[0.00700690485237615 0.4765]
MF3='in2mf3':'gaussmf',
[0.00700690485237615 0.493]
```

```
[Input3]
Name='XM'
Range=[124.792 144.942]
NumMFs=3
MF1='in3mf1':'gaussmf',
[4.2784585689509 124.792]
MF2='in3mf2':'gaussmf',
[4.2784585689509 134.867]
MF3='in3mf3':'gaussmf',
[4.2784585689509 144.942]
```

```
[Input4]
Name='YM'
Range=[310.931 326.784]
NumMFs=3
MF1='in4mf1':'gaussmf',
[3.36607462499149 310.931]
MF2='in4mf2':'gaussmf',
[3.36607462499149 318.8575]
MF3='in4mf3':'gaussmf',
[3.36607462499149 326.784]
```

```
[Input5]
Name='IntDen'
Range=[99164 118792]
NumMFs=3
MF1='in5mf1':'gaussmf',
[4167.62207401331 99164]
MF2='in5mf2':'gaussmf',
[4167.62207401331 108978]
MF3='in5mf3':'gaussmf',
[4167.62207401331 118792]
```

```
[Input6]
Name='Skew'
Range=[-0.856 -0.331]
NumMFs=3
MF1='in6mf1':'gaussmf',
[0.111473486287802 -0.856]
MF2='in6mf2':'gaussmf',
[0.111473486287802 -0.5935]
MF3='in6mf3':'gaussmf',
[0.111473486287802 -0.331]
```

```
[Input7]
Name='Kurt'
Range=[-1.89 -1.267]
NumMFs=3
MF1='in7mf1':'gaussmf',
[0.132281870394859 -1.89]
MF2='in7mf2':'gaussmf',
[0.132281870394859 -1.5785]
MF3='in7mf3':'gaussmf',
[0.132281870394859 -1.267]
```

```
[Input8]
Name='Areap'
Range=[58.162 69.674]
NumMFs=3
MF1='in8mf1':'gaussmf',
[2.44434814122892 58.162]
MF2='in8mf2':'gaussmf',
[2.44434814122892 63.918]
MF3='in8mf3':'gaussmf',
[2.44434814122892 69.674]
```

2) OUTPUT MEMBERSHIP FUNCTIONS

```
MF1='out1mf1':'constant', [0]
MF2='out1mf2':'constant', [0]
MF3='out1mf3':'constant', [0]
MF4='out1mf4':'constant', [0]
MF5='out1mf5':'constant', [0]
MF6='out1mf6':'constant', [0]
MF7='out1mf7':'constant', [0]
MF8='out1mf8':'constant', [0]
MF9='out1mf9':'constant', [0]
MF10='out1mf10':'constant', [0]
```

B. FUZZY RULES

After the fuzzification process, rule generation will start. The degree of fuzzification of input membership functions is known to algorithms in which each part of the antecedent has been satisfied for each rule. It is necessary to apply the fuzzy operator (for example OR, AND) if the given rule has more than one part which yields one number that represents the result of the antecedent for that rule. This number will then be applied to the output function. The input to the fuzzy operator is two or more membership values from fuzzified input variables. The output is a single truth value. The following listing will give some set of rules incorporating the fuzzy operators. Fig. 28 gives corresponding graphical representation of rules shown in following listing.

- Rule 1. $\text{if}(\text{Mean} \in \text{in1mf1}) \wedge \text{if}(\text{SD} \in \text{in2mf1}) \wedge \text{if}(\text{XM} \in \text{in3mf1}) \wedge \text{if}(\text{YM} \in \text{in4mf2}) \wedge \text{if}(\text{IntDen} \in \text{in5mf1}) \wedge \text{if}(\text{Skew} \in \text{in6mf2}) \wedge \text{if}(\text{Kurt} \in \text{in7mf2}) \wedge \text{if}(\text{Areap} \in \text{in8mf2}) \implies (\text{output}=\text{out1mf1})(1)$
- Rule 2. $\text{if}(\text{Mean} \notin \text{in1mf1}) \wedge \text{if}(\text{SD} \notin \text{in2mf1}) \wedge \text{if}(\text{XM} \in \text{in3mf1}) \wedge \text{if}(\text{YM} \in \text{in4mf2}) \wedge \text{if}(\text{IntDen} \notin \text{in5mf1}) \wedge \text{if}(\text{Skew} \in \text{in6mf3}) \wedge \text{if}(\text{Kurt} \in \text{in7mf1}) \wedge \text{if}(\text{Areap} \in \text{in8mf2}) \implies (\text{output}=\text{out1mf2})(1)$
- Rule 3. $\text{if}(\text{Mean} \in \text{in1mf1}) \wedge \text{if}(\text{SD} \in \text{in2mf2}) \wedge \text{if}(\text{XM} \in \text{in3mf2}) \wedge \text{if}(\text{YM} \in \text{in4mf2}) \wedge \text{if}(\text{IntDen} \in \text{in5mf2}) \wedge \text{if}(\text{Skew} \in \text{in6mf3}) \wedge \text{if}(\text{Kurt} \in \text{in7mf3}) \wedge \text{if}(\text{Areap} \in \text{in8mf3}) \implies (\text{output}=\text{out1mf3})(1)$
- Rule 4. $\text{if}(\text{Mean} \in \text{in1mf1}) \wedge \text{if}(\text{SD} \in \text{in2mf2}) \wedge \text{if}(\text{XM} \in \text{in3mf2}) \wedge \text{if}(\text{YM} \in \text{in4mf2}) \wedge \text{if}(\text{IntDen} \in \text{in5mf3}) \wedge \text{if}(\text{Skew} \in \text{in6mf1}) \wedge \text{if}(\text{Kurt} \in \text{in7mf1}) \wedge \text{if}(\text{Areap} \in \text{in8mf1}) \implies (\text{output}=\text{out1mf4})(1)$

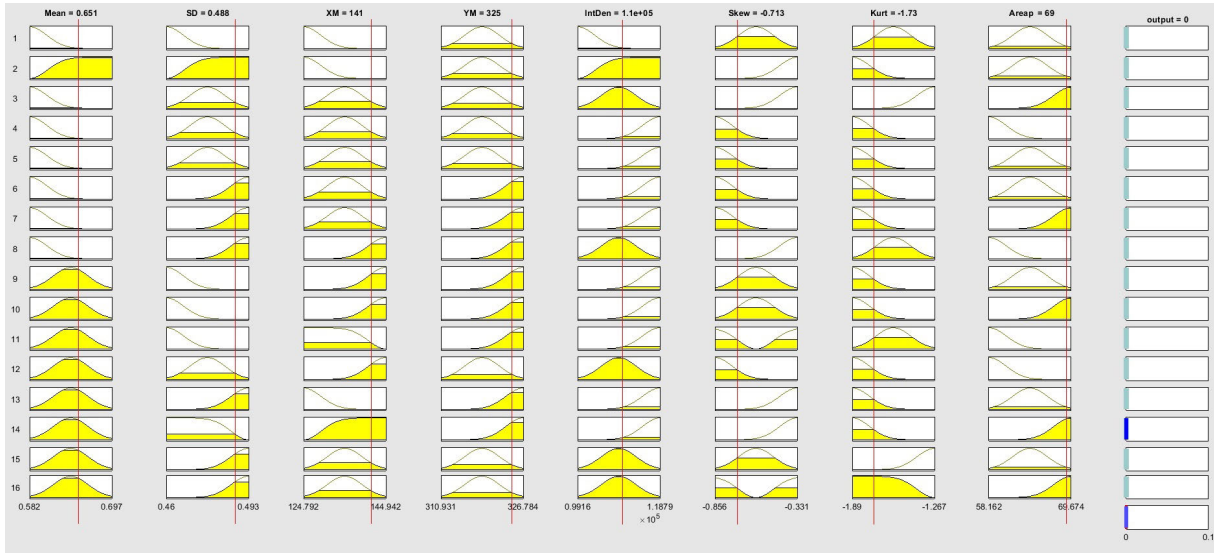


FIGURE 28. Graphical representation of fuzzy rules shown in listing.

- Rule 5. $\text{if}(\text{Mean} \in \text{in1mf1}) \wedge \text{if}(\text{SD} \in \text{in2mf2}) \wedge \text{if}(\text{XM} \in \text{in3mf2}) \wedge \text{if}(\text{YM} \in \text{in4mf2}) \wedge \text{if}(\text{IntDen} \in \text{in5mf3}) \wedge \text{if}(\text{Skew} \in \text{in6mf1}) \wedge \text{if}(\text{Kurt} \in \text{in7mf1}) \wedge \text{if}(\text{Areap} \in \text{in8mf2}) \Rightarrow (\text{output}=\text{out1mf5})(1)$
- Rule 6. $\text{if}(\text{Mean} \in \text{in1mf1}) \wedge \text{if}(\text{SD} \in \text{in2mf3}) \wedge \text{if}(\text{XM} \in \text{in3mf2}) \wedge \text{if}(\text{YM} \in \text{in4mf3}) \wedge \text{if}(\text{IntDen} \in \text{in5mf3}) \wedge \text{if}(\text{Skew} \in \text{in6mf1}) \wedge \text{if}(\text{Kurt} \in \text{in7mf1}) \wedge \text{if}(\text{Areap} \in \text{in8mf2}) \Rightarrow (\text{output}=\text{out1mf6})(1)$
- Rule 7. $\text{if}(\text{Mean} \in \text{in1mf1}) \wedge \text{if}(\text{SD} \in \text{in2mf3}) \wedge \text{if}(\text{XM} \in \text{in3mf2}) \wedge \text{if}(\text{YM} \in \text{in4mf3}) \wedge \text{if}(\text{IntDen} \in \text{in5mf3}) \wedge \text{if}(\text{Skew} \in \text{in6mf1}) \wedge \text{if}(\text{Kurt} \in \text{in7mf1}) \wedge \text{if}(\text{Areap} \in \text{in8mf3}) \Rightarrow (\text{output}=\text{out1mf7})(1)$
- Rule 8. $\text{if}(\text{Mean} \in \text{in1mf1}) \wedge \text{if}(\text{SD} \in \text{in2mf3}) \wedge \text{if}(\text{XM} \in \text{in3mf3}) \wedge \text{if}(\text{YM} \in \text{in4mf3}) \wedge \text{if}(\text{IntDen} \in \text{in5mf2}) \wedge \text{if}(\text{Skew} \in \text{in6mf3}) \wedge \text{if}(\text{Kurt} \in \text{in7mf2}) \wedge \text{if}(\text{Areap} \in \text{in8mf1}) \Rightarrow (\text{output}=\text{out1mf8})(1)$
- Rule 9. $\text{if}(\text{Mean} \in \text{in1mf2}) \wedge \text{if}(\text{SD} \in \text{in2mf1}) \wedge \text{if}(\text{XM} \in \text{in3mf3}) \wedge \text{if}(\text{YM} \in \text{in4mf3}) \wedge \text{if}(\text{IntDen} \in \text{in5mf3}) \wedge \text{if}(\text{Skew} \in \text{in6mf2}) \wedge \text{if}(\text{Kurt} \in \text{in7mf1}) \wedge \text{if}(\text{Areap} \in \text{in8mf2}) \Rightarrow (\text{output}=\text{out1mf9})(1)$
- Rule 10. $\text{if}(\text{Mean} \in \text{in1mf2}) \wedge \text{if}(\text{SD} \in \text{in2mf1}) \wedge \text{if}(\text{XM} \in \text{in3mf3}) \wedge \text{if}(\text{YM} \in \text{in4mf3}) \wedge \text{if}(\text{IntDen} \in \text{in5mf3}) \wedge \text{if}(\text{Skew} \in \text{in6mf2}) \wedge \text{if}(\text{Kurt} \in \text{in7mf1}) \wedge \text{if}(\text{Areap} \in \text{in8mf3}) \Rightarrow (\text{output}=\text{out1mf10})(1)$
- Rule 11. $\text{if}(\text{Mean} \in \text{in1mf2}) \wedge \text{if}(\text{SD} \in \text{in2mf1}) \wedge \text{if}(\text{XM} \notin \text{in3mf3}) \wedge \text{if}(\text{YM} \in \text{in4mf3}) \wedge \text{if}(\text{IntDen} \in \text{in5mf3}) \wedge \text{if}(\text{Skew} \notin \text{in6mf2}) \wedge \text{if}(\text{Kurt} \in \text{in7mf2}) \wedge \text{if}(\text{Areap} \in \text{in8mf1}) \Rightarrow (\text{output}=\text{out1mf11})(1)$
- Rule 12. $\text{if}(\text{Mean} \in \text{in1mf2}) \wedge \text{if}(\text{SD} \in \text{in2mf2}) \wedge \text{if}(\text{XM} \in \text{in3mf3}) \wedge \text{if}(\text{YM} \in \text{in4mf2}) \wedge \text{if}(\text{IntDen} \in \text{in5mf2}) \wedge \text{if}(\text{Skew} \in \text{in6mf1}) \wedge \text{if}(\text{Kurt} \in \text{in7mf1}) \wedge \text{if}(\text{Areap} \in \text{in8mf1}) \Rightarrow (\text{output}=\text{out1mf12})(1)$
- Rule 13. $\text{if}(\text{Mean} \in \text{in1mf2}) \wedge \text{if}(\text{SD} \in \text{in2mf3}) \wedge \text{if}(\text{XM} \in \text{in3mf1}) \wedge \text{if}(\text{YM} \in \text{in4mf3}) \wedge \text{if}(\text{IntDen} \in \text{in5mf3}) \wedge \text{if}(\text{Skew} \in \text{in6mf3}) \wedge \text{if}(\text{Kurt} \in \text{in7mf1}) \wedge \text{if}(\text{Areap} \in \text{in8mf2}) \Rightarrow (\text{output}=\text{out1mf13})(1)$
- Rule 14. $\text{if}(\text{Mean} \in \text{in1mf2}) \vee \text{if}(\text{SD} \notin \text{in2mf3}) \vee \text{if}(\text{XM} \notin \text{in3mf1}) \vee \text{if}(\text{YM} \in \text{in4mf3}) \vee \text{if}(\text{IntDen} \in \text{in5mf3}) \vee \text{if}(\text{Skew} \in \text{in6mf3}) \vee \text{if}(\text{Kurt} \in \text{in7mf1}) \vee \text{if}(\text{Areap} \in \text{in8mf3}) \Rightarrow (\text{output}=\text{out1mf14})(1)$
- Rule 15. $\text{if}(\text{Mean} \in \text{in1mf2}) \wedge \text{if}(\text{SD} \in \text{in2mf3}) \wedge \text{if}(\text{XM} \in \text{in3mf2}) \wedge \text{if}(\text{YM} \in \text{in4mf2}) \wedge \text{if}(\text{IntDen} \in \text{in5mf2}) \wedge \text{if}(\text{Skew} \in \text{in6mf2}) \wedge \text{if}(\text{Kurt} \in \text{in7mf3}) \wedge \text{if}(\text{Areap} \in \text{in8mf2}) \Rightarrow (\text{output}=\text{out1mf15})(1)$
- Rule 16. $\text{if}(\text{Mean} \in \text{in1mf2}) \wedge \text{if}(\text{SD} \in \text{in2mf3}) \wedge \text{if}(\text{XM} \in \text{in3mf2}) \wedge \text{if}(\text{YM} \in \text{in4mf2}) \wedge \text{if}(\text{IntDen} \in \text{in5mf2}) \wedge \text{if}(\text{Skew} \notin \text{in6mf2}) \wedge \text{if}(\text{Kurt} \notin \text{in7mf3}) \wedge \text{if}(\text{Areap} \in \text{in8mf3}) \Rightarrow (\text{output}=\text{out1mf16})(1)$

C. AGGREGATE ALL OUTPUTS

All the fuzzy rules need to combine to make a decision. The process of combining the output of each rule into a single fuzzy set to get a resolution is known as aggregation. The rules are combined using probabilistic OR method, maximum method, or summation of each rule of a fuzzy output set. Aggregation occurs once for each output variable, just before the defuzzification. In the aggregation process, the input is the list of pruned output features returned for each rule by the

implication method. A fuzzy set for each output variable is the output of the aggregation process.

D. DEFUZZIFICATION

The fuzzy logic starts with converting a crisp set into a fuzzy set. Then fuzzy membership function will be created based on linguistics. Finally, the defuzzification will be done. Defuzzification is an essential process to produce the fuzzy quantifiable result in crisp logic. In other words, it is a mapping of fuzzy set into a crisp set. For this research, the output membership function obtained using FKNN, FSVM, and FESD are symmetrical; therefore, the weighted-average method of defuzzification has been applied. This method is also known as Sugeno defuzzification method. For this purpose, the crisp values can be obtained from Eq. 7.

$$X^* = \frac{\sum_{i=1}^n \mu_{C_i}(X_i) \cdot (X_i)}{\sum_{i=1}^n \mu_{C_i}(X_i)} \quad (7)$$

where, C_1, C_2, \dots, C_n are the output fuzzy sets and (X_i) is the value where centre of the fuzzy set C_i is observed.

E. GRID PARTITIONING

The grid partitioning fuzzy inference system as shown in Fig. 29, consists of 8 input features and one output. Table 9 shows feature space corresponding to input feature. The name of this FIS is *footGP*. [57] gives Sugano FIS model, which generates a sum of 1296 rules. The fuzzy operator AND method is the product of fuzzified input values, while fuzzy operator OR follows probabilistic OR of fuzzified input values. Implication method for computing resulting fuzzy set in this approach follows product as scale the resultant membership function by the predecessor result value. Sum of following fuzzy sets defines the aggregation method. Crisp output values have figured during the defuzzification phase

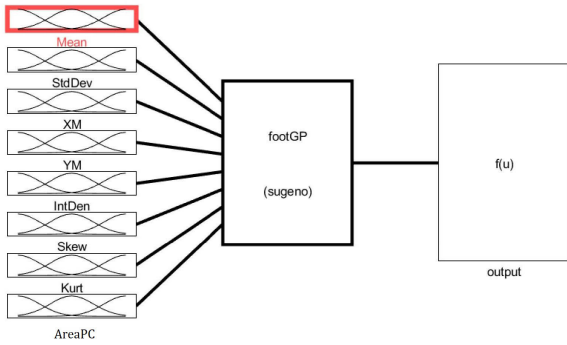


FIGURE 29. Sugano FIS for footprint dataset for 8 input features and 1 output.

TABLE 9. Attribute range of 8 normalized extracted features (Grid Partitioning).

Features	Range
Mean	[0.582 0.697]
StdDev	[0.46 0.493]
XM	[124.792 144.942]
YM	[310.931 326.784]
IntDen	[99164 118792]
Skew	[-0.856 -0.331]
Kurt	[-1.89 -1.267]
Area%	[58.162 69.674]

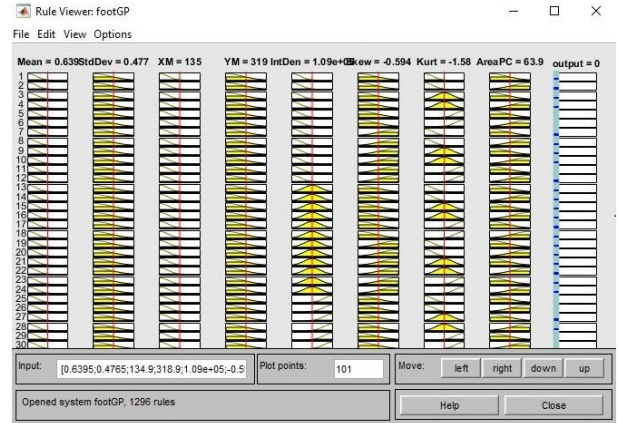


FIGURE 31. Graphical representation of fuzzy rules.

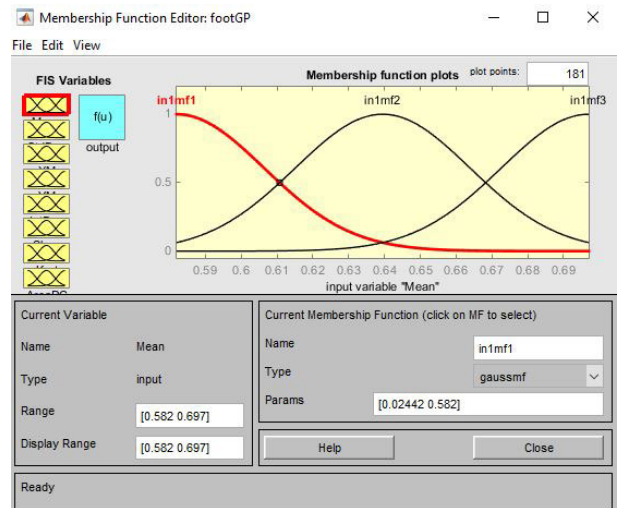


FIGURE 32. Membership plot for feature Mean.

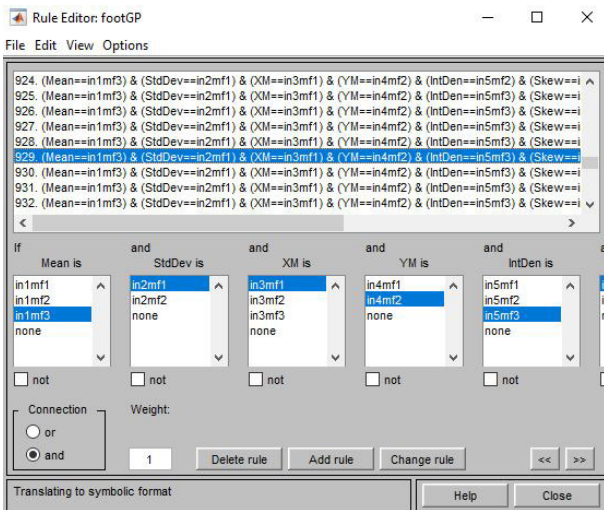


FIGURE 30. Sample fuzzy rules in verbose mode.

by the weighted average of all rule outputs. Fig. 30-33, shows grid partitioned Sugano FIS. In these figures, Fig. 30 shows sample fuzzy rules in verbose mode, Fig. 31 gives the graphical representation of fuzzy rules, Fig. 32 shows a membership plot for feature Mean, and Fig. 33 shows the surface plot between StdDev, Mean, and Output Class.

F. SUBSPACE CLUSTERING

The Subspace Clustering based fuzzy inference system shown in Fig. 34, consists of 8 input features and one output.

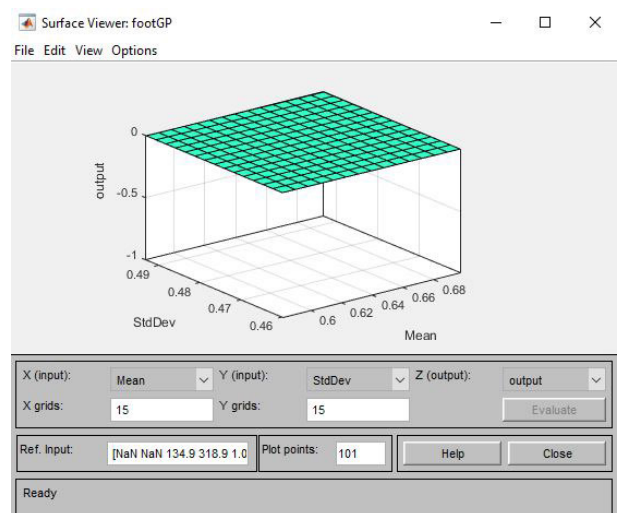


FIGURE 33. Surface plot between StdDev, Mean, Output Class.

Table 10 shows feature space corresponding to input feature. The name of this FIS is *footSC*. The Sugano based model generates a sum of 9 rules. The fuzzy operator AND method

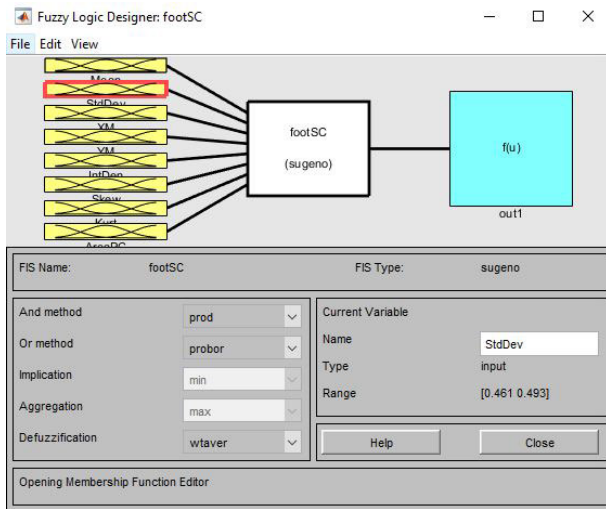


FIGURE 34. Subspace clustered Sugano FIS :Sugano FIS for footprint dataset for 8 input features and 1 output.

TABLE 10. Attribute range of 8 normalized extracted features (Subspace Partitioning).

Features	Range
Mean	[0.585 0.694]
StdDev	[0.461 0.493]
XM.	[124.804 144.73]
YM	[310.931 322.059]
IntDen	[99818 118243]
Skew	[-0.84 -0.347]
Kurt	[-1.88 -1.295]
Area%	[58.546 69.352]

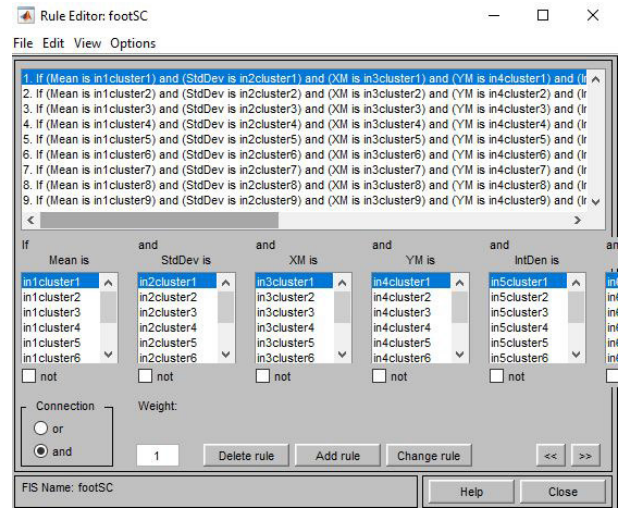


FIGURE 36. Fuzzy rules in verbose mode.



FIGURE 37. Graphical representation of fuzzy rules.

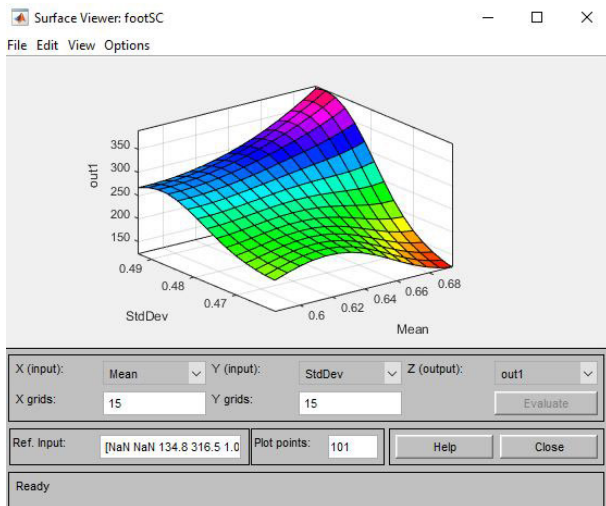


FIGURE 35. Surface plot between StdDev, Mean, Output Class.

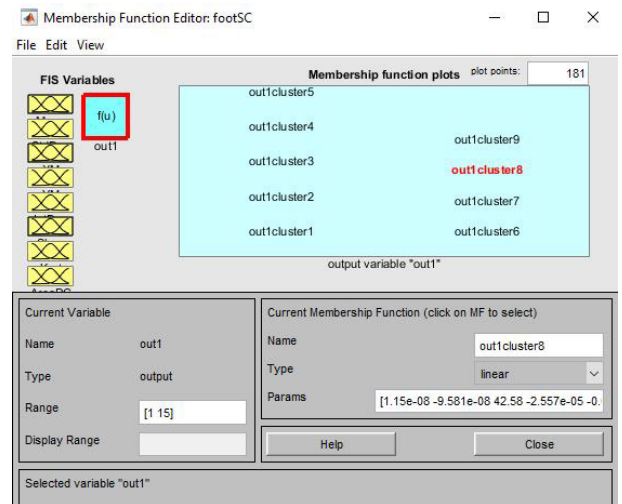


FIGURE 38. Membership plot of output MF out1.

is the product of a fuzzified input values, while fuzzy operator OR follows probabilistic OR of fuzzified input values. Implication method for computing resulting fuzzy set in this approach follows product as scale the resultant membership function by the predecessor result value. Maximum of

following fuzzy sets defines the aggregation method. Crisp output values have figured during the defuzzification phase by the weighted average of all rule outputs. Fig. 34-39, shows

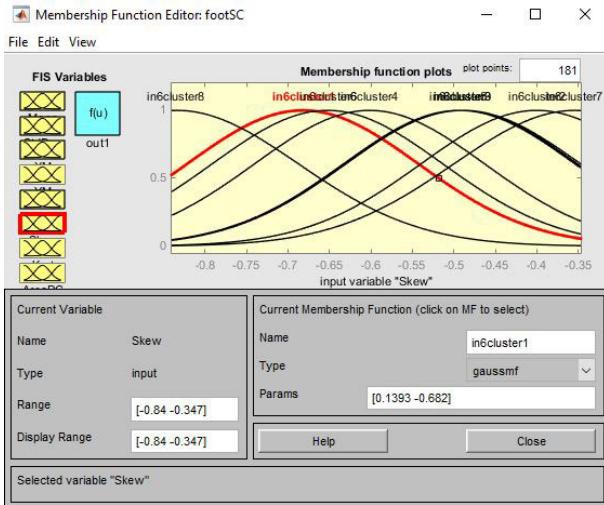


FIGURE 39. Membership plot of input MF Skew.

subspace clustered Sugano FIS. Fig.34 shows Sugano FIS for footprint dataset for 8 input features and 1 output. The surface plot between *StdDev*, *Mean*, *Output Class* is shown in Fig. 35. Fig. 36 and Fig. 37 shows fuzzy rules in verbose mode, and graphical mode respectively. Fig. 38 and Fig. 39 gives the membership plot for output MF *out1*, and input MF *Skew* respectively.

Fig. 40 give the brief idea about proposed approach. The algorithm strat with capturing the data then splitting the dataset and finally evaluated through FKNN, FSVM, and FESD approach.

APPENDIX B FINE GAUSSIAN SVM (Fuzzy Kernel) FOOTPRINT MATCHER

The accuracy is very important in any matching algorithm. The Support Vector Machine has tremendous learning abilities for such kind of classification and match. The SVM kernel is a mathematical function that transform input feature space into desired forms. The coordinates of the training set closest to classifying hyperplane defines support vectors. The classifying hyperplane has a scope of maximum margin both side; it can classify both linear and non-linear problems with sporadic chances of overfitting. The transformation of datapoint from non-linear space to linear space gives kernel trick. Suppose, $K(p, q) = \langle f(p), f(q) \rangle$, is a kernel function over n-dimensional feature space p and q , then f is a function that maps high-dimensional feature space to optimized m-dimension feature space ($f : n \mapsto m$). The Gaussian kernel $K(p, q)$ with the parameter $\gamma > 0$, shown in Eq. 8, is used with the intention of no prior knowledge of input (most of the literature used $\gamma = 1/(2\sigma^2)$).

$$K(p, q) = e^{-\gamma \|p-q\|^2} \quad (8)$$

The FSVM method shown in Algo. 3, is the combination of fuzzy classifiers and Gaussian kernel machine aiming to

Algorithm 3 Footprint Matcher: Fine Gaussian SVM (Fuzzy Kernel)

Require: input test sets \vec{x} , and \vec{y}

Require: initial output membership function out_0

Require: location parameter z_j^k ;
{ Construct Gaussian Kernel }

for $j:=1$ to m **do**

for $k:=1$ to n **do**

$K(\vec{x}, z_j) \leftarrow K(\vec{x}, z_{j-1}) \times in^k(x_k - z_j^k)$
{ The Gaussian membership function }

$\mu(x) \leftarrow e^{-\gamma x^2}; \forall \gamma > 0$

{ transformed to Fourier transform }

$F[\mu](\omega) \leftarrow \frac{1}{\sqrt{2\gamma}} e^{-\frac{\omega^2}{4\gamma}}$

end for

end for

$t_0 \leftarrow 0$

$out_0 \leftarrow 0$

$j \leftarrow 1$

for $i:=1$ to p **do**

for $j:=1$ to p **do**

$maximize \quad G(\vec{\eta}) \quad \leftarrow \quad \sum_{i=1}^p \eta_i$
 $\frac{1}{2} \sum_{i=j=1}^p \eta_i \eta_j y_i y_j K(\vec{x}, \vec{x}_j)$
subject to $0 \leq \eta_i \leq 1$;

end for

$t_i \leftarrow t_{i-1} + y_i \eta_i$ {Final value of t_i must be unity.}

if $\eta_i > 0$ **then**

$\vec{z}_j \leftarrow \vec{x}_i$

$out_j \leftarrow y_i \eta_i$

$j \leftarrow j + 1$

end if

$m \leftarrow j - 1$

end for

find optimum values for cost function and kernel parameter to achieve a best footprint match with a low error rate. FSVM as a unique classification model with powerful generalization capability, robustness, and good interpretability resembles to be a promising approach for biometric footprint matching. The feature set consists of a large set of features for 6 samples per footprint of 220 volunteers. Consider a fuzzy rule from grid partitioning method as shown in 9.

Rule 6 : If (*Mean* == *in1mf1*) \wedge

(*StdDev* == *in2mf1*) \wedge (*XM* == *in3mf1*)

\wedge (*YM* == *in4mf1*) \wedge (*IntDen* == *in5mf1*)

\wedge (*Skew* == *in6mf1*) \wedge (*Kurt* == *in7mf3*)

\wedge (*AreaPC* == *in8mf2*) then (*output* == *out1mf6*)

(9)

This rule can also be written in general form as shown in 10.

Rule j : IF $in_j^1 \wedge in_j^2 \wedge in_j^3 \dots \wedge in_j^n$ THEN out_j (10)

where, for any fuzzy implication R , the output membership function $out_j \in R$, and IN_j^k is the fuzzy set with input

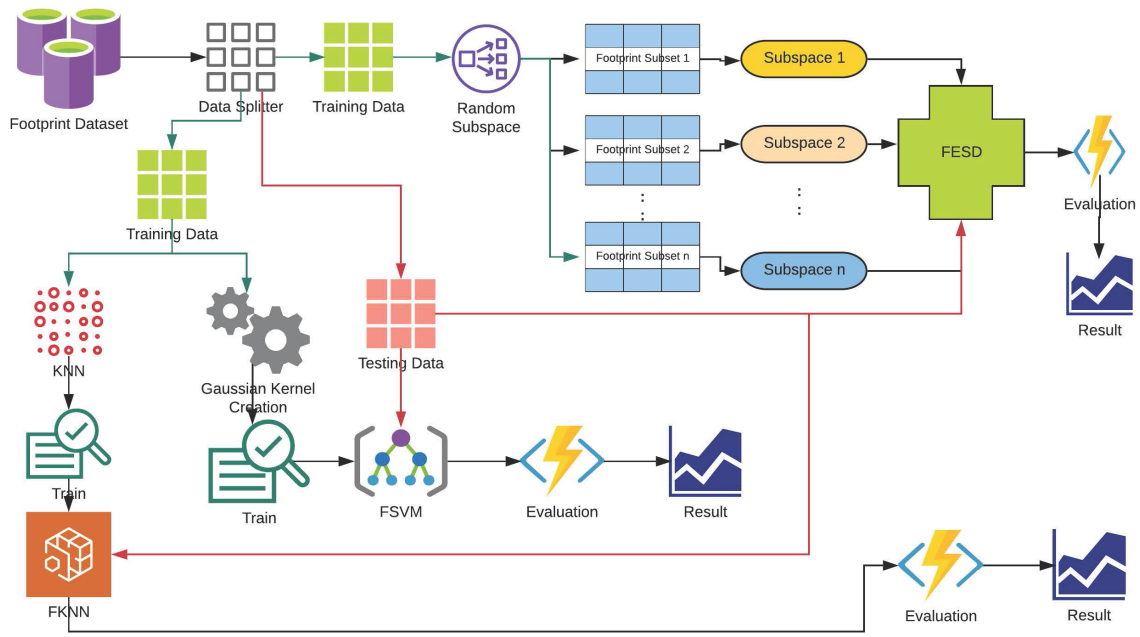


FIGURE 40. Summarize view of FSVM, FKNN, and FESD algorithm.

membership function $in_j^k : R \mapsto [0, 1], \forall j = 1, 2, \dots, m$, and $\forall k = 1, 2, \dots, n$. Here for this purpose, the grid portioning model presented in subsection A-E is required. For any input feature space $\vec{x} = [x_1, x_2, \dots, x_n]^T$, the input to output mapping $F : R^n \mapsto R$ is defined by Eq. 11.

$$F(\vec{x}) = \frac{\sum_{j=1}^m out_j \prod_{k=1}^n in_j^k(x_k)}{\sum_{j=1}^m \prod_{k=1}^n in_j^k(x_k)} \quad (11)$$

It might be possible that the feature space is not able to cover all the rules. Then Rule 0 could be added by using Eq. 10, alternatively, the Eq. 11 transformed into Eq. 12.

$$F(\vec{x}) = \frac{out_0 + \sum_{j=1}^m out_j \prod_{k=1}^n in_j^k(x_k)}{1 + \sum_{j=1}^m \prod_{k=1}^n in_j^k(x_k)} \quad (12)$$

Now, it is important to find the incorrect or negative data from the input output training pair. the sign of Eq. 12 determines the positive and negative samples shown by a classifier $Label(\vec{x})$, in eq 13. A second form can also be productive because the only numerator is responsible for returning the sign. After knowing the sign of function F , next step is to apply Gaussian Kernel into the SVM. Because the SVM narrows the scope of F , generated from a membership function μ defined on the footprint matcher. This membership function become reference function if Eq. 14 satisfies. For a given location parameter z_j^k , following property of location transformation holds in Eq. 15. Then, the Eq. 16 gives the transform invariant Gaussian Kernel. Thereafter, the Eq. 13, will now converted to Eq. 17

$$Label(\vec{x}) = sign(F(\vec{x})) = sign(out_0 + \sum_{j=1}^m out_j \prod_{k=1}^n in_j^k(x_k)) \quad (13)$$

$$\mu(x) = \mu(-x) \text{ and } \mu(0) = 1 \quad (14)$$

$$in_j^k(x_k) = in_j^k(x_k - z_j^k); \quad \forall z_j^k \in R \quad (15)$$

$$\left. \begin{aligned} K(\vec{x}, z_j) &= \prod_{k=1}^n in_j^k(x_k - z_j^k) \\ \text{The Gaussian} \\ \text{membership function } \mu(x) &= e^{-\gamma x^2}; \quad \gamma > 0 \\ \text{transformed to Fourier transform } F[\mu](\omega) &= \frac{1}{\sqrt{2\gamma}} e^{-\frac{\omega^2}{4\gamma}} \end{aligned} \right\} \quad (16)$$

$$Label(\vec{x}) = sign(out_0 + \sum_{j=1}^m out_j K(\vec{x}, \vec{z}_j)) \quad (17)$$

For another set of training input $\vec{y} = [y_1, y_2, \dots, y_p]$, and SVM learning parameter $\vec{\eta}$, maximization of classified matching footprint feature points could be given as Eq. 18.

$$\begin{aligned} \text{maximize } G(\vec{\eta}) &= \sum_{i=1}^p \eta_i - \frac{1}{2} \sum_{i=j=1}^p \eta_i \eta_j y_i y_j K(\vec{x}, \vec{x}_j) \\ \text{subject to } &0 \leq \eta_i \leq 1; \quad \forall i = 1, \dots, p; \quad \text{and } \sum_{i=1}^p y_i \eta_i = 1 \end{aligned} \quad (18)$$

$$f(\vec{x}) = sign(out_0 + \sum_{j=1}^m \eta_j y_j K(\vec{x}, \vec{x}_j)) \quad (19)$$

Finally, from unknown values to given known values, the 2 input training sets, the SVM learning parameter, and the initial value of output membership function, upon solving Eq. 18 which is related to Eq. 17, the classes of positive match and negative match will be given by Eq. 19.

APPENDIX C

FINE KNN BASED FOOTPRINT MATCHER

The KNN follows straightforward approach. The training dataset is helpful to award a class from new cases based on a similarity value of k nearest neighbors. The problem may arise, how to find the minimum distances between the subject and neighbors. This algorithm follows two-step approach, viz. the first step is to calculate the similarity based on distance functions $d(x, y)$. For p different points, x_i , and y_i , the Euclidean distance can be calculated by Eq. 20, and Eq. 21 calculates distance by Manhattan function.

$$d_e(x, y) = \sqrt{\sum_{i=1}^p (x_i - y_i)^2} \quad (20)$$

$$d_m(x, y) = \sum_{i=1}^p \|x_i - y_i\| \quad (21)$$

Here, this idea could use to find, how two or more footprints are similarly based on eight listed features. The second step is involved in finding the distances for k-nearest neighbors. Based on minimum distances often called rank, the subject (here footprint) awarded by the nearest class value. The footprint dataset consists of parameters of different units. This is important to standardize the features to find the similarity score of the diverse set of footprints. Sometimes, it is also possible the features of the test class may match with 2 or more classes due to confusion, often known as an outlier. The value of outliers also plays a vital role in finding the matching rate of footprints [58].

Algorithm 4 Footprint Matcher: Fine KNN

Require: Input unknown footprint x
 {Set $K : 1 \leq K \leq n$ }
for $i:=1$ to n **do**
 Find minimum distance $d_e(x, x_i) \leftarrow$
 $\min\left(\sqrt{\sum_{i=1}^n (x - x_i)^2}\right)$
 if $i < K$ **then**
 $add(x_i)$ in set of K-nearest neighbors
 else if x_i is closer than x_{i-1} **then**
 $delete(x_{i-1})$ from set of K-nearest neighbors
 $add(x_i)$ in set of K-nearest neighbors
 end if
end for
 $i \leftarrow 1$
repeat
 $\mu_i(x) \leftarrow \frac{\sum_{j=1}^K \mu_i(x_j) d_e(x, x_j)^{-2/(m-1)}}{\sum_{j=1}^K d_e(x, x_j)^{-2/(m-1)}}$
 $i \leftarrow i + 1$
until x assigned membership in all classes

The Algo. 4, is described as follows. Let, $\omega = \{x_1, x_2, \dots, x_n\}$, be the set of labeled footprint samples. The assigned membership of unknown footprint vector x is given by $\mu_i(x)$. The μ_{ij} , computes the membership of i^{th} class of j^{th}

vector of ω . The $\mu_i(x)$ can be computed by Eq. 22, is determined by the inverse of distances from their nearest neighbors and their class membership. The highest membership value has awarded upon determining all the memberships for a test footprint sample.

$$\mu_i(x) = \frac{\sum_{j=1}^K \mu_i(x_j) d_e(x, x_j)^{-2/(m-1)}}{\sum_{j=1}^K d_e(x, x_j)^{-2/(m-1)}}$$

or, by:
$$\mu_i(x) = \frac{\sum_{j=1}^K \mu_{ij} (1/\|x - x_j\|^{-2/(m-1)})}{\sum_{j=1}^K (1/\|x - x_j\|^{-2/(m-1)})} \quad (22)$$

This algorithm follows fine grain partitioning. The success rate of FKNN depends on the value m , is a weighing factor to determining the contribution of each neighbors to the membership values. Typically m ranges from 1.5 to 2.5 for better result. As the value of $m > 1$, the membership values gradually increases.

REFERENCES

- [1] A. K. Jain, Y. Chen, and M. Demirkus, "Pores and ridges: High-resolution fingerprint matching using level 3 features," *IEEE Trans. Pattern Anal. Mach. Intell.*, vol. 29, no. 1, pp. 15–27, Jan. 2007.
- [2] G. R. Sinha and P. S. Oo, *Introduction to Biometrics and Special Emphasis on Myanmar Sign Language Recognition*. Cham, Switzerland: Springer, 2019, pp. 1–23, doi: 10.1007/978-3-030-30436-2_1.
- [3] G. Sinha and S. Patil, *Biometrics: Concepts and Applications*. Hoboken, NJ, USA: Wiley, 2013.
- [4] P. Wild, "Single-sensor hand and footprint-based multimodal biometric recognition," M.S. thesis, Dept. Natural Sci., Univ. Salzburg, Salzburg, Austria, Jan. 2008. [Online]. Available: <http://wavelab.at/papers/Wild08a.pdf>
- [5] V. L. Naples and J. S. Miller, "Making tracks: The forensic analysis of footprints and footwear impressions," *Anatomical Rec.*, vol. 279B, no. 1, pp. 9–15, Jul. 2004, doi: 10.1002/ar.b.20025.
- [6] K. Nakajima, Y. Mizukami, K. Tanaka, and T. Tamura, "Footprint-based personal recognition," *IEEE Trans. Biomed. Eng.*, vol. 47, no. 11, pp. 1534–1537, Nov. 2000.
- [7] J.-W. Jung, K.-H. Park, and Z. Bien, *Unconstrained Person Recognition Method using Dynamic Footprint*, vol. 25. Washington, DC, USA: The Institute of Electronics Engineers of Korea, 2002, pp. 91–94. [Online]. Available: <http://www.dbpia.co.kr/Article/NODE06328878>
- [8] J. W. Jung, J. S. Han, T. Sato, and Z. Bien, *Unconstrained Person Recognition Method Using Dynamic Partial Footprints From Floor-Type Pressure Sensor*. Washington, DC, USA: The Institute of Electronics Engineers of Korea, 2003, pp. 85–88. [Online]. Available: <http://www.dbpia.co.kr/Article/NODE01742196>
- [9] J.-W. Jung, Z. Bien, S.-W. Lee, and T. Sato, "Dynamic-footprint based person identification using mat-type pressure sensor," in *Proc. 25th Annu. Int. Conf. IEEE Eng. Med. Biol. Soc.*, Sep. 2003, pp. 2937–2940.
- [10] J.-W. Jung, T. Sato, and Z. Bien, "Dynamic footprint-based person recognition method using a hidden Markov model and a neural network," *Int. J. Intell. Syst.*, vol. 19, no. 11, pp. 1127–1141, Nov. 2004, doi: 10.1002/int.20040.
- [11] J. Yun, G. Abowd, W. Woo, and J. Ryu, "Biometric user identification with dynamic footprint," in *Proc. 2nd Int. Conf. Bio-Inspired Comput., Theories Appl.*, Sep. 2007, pp. 225–230.
- [12] A. Uhl and P. Wild, "Personal identification using eigenfeet, ballprint and foot geometry biometrics," in *Proc. 1st IEEE Int. Conf. Biometrics, Theory, Appl., Syst.*, Sep. 2007, pp. 1–6.
- [13] A. Uhl, "Footprint-based biometric verification," *J. Electron. Imag.*, vol. 17, no. 1, Jan. 2008, Art. no. 011016, doi: 10.1117/1.2892674.
- [14] K. Krishan, "Estimation of stature from footprint and foot outline dimensions in gujjars of north india," *Forensic Sci. Int.*, vol. 175, nos. 2–3, pp. 93–101, Mar. 2008. [Online]. Available: <http://www.sciencedirect.com/science/article/pii/S0379073807005415>

- [15] T. Nataraja Moorthy and S. F. B. Sulaiman, "Individualizing characteristics of footprints in Malaysian Malays for person identification from a forensic perspective," *Egyptian J. Forensic Sci.*, vol. 5, no. 1, pp. 13–22, Mar. 2015. [Online]. Available: <http://www.sciencedirect.com/science/article/pii/S2090536X14000240>
- [16] T. Takeda, K. Taniguchi, K. Asari, K. Kuramoto, S. Kobashi, and Y. Hata, "Biometric personal authentication by one step foot pressure distribution change by load distribution sensor," in *Proc. IEEE Int. Conf. Fuzzy Syst.*, Aug. 2009, pp. 906–910.
- [17] T. Takeda, K. Kuramoto, S. Kobashi, and Y. Hata, "Biometric personal authentication by one step foot pressure distribution change by fuzzy artificial immune system," in *Proc. Int. Conf. Fuzzy Syst.*, Jul. 2010, pp. 1–6.
- [18] T. Takeda, K. Kuramoto, S. Kobashi, and Y. Hata, "Fuzzy-logic is precise—Its application to biometric system," *Scientia Iranica*, vol. 18, no. 3, pp. 655–662, Jun. 2011. [Online]. Available: <http://www.sciencedirect.com/science/article/pii/S102630981100068X>
- [19] H. Ye, S. Kobashi, Y. Hata, K. Taniguchi, and K. Asari, "Biometric system by foot pressure change based on neural network," in *Proc. 39th Int. Symp. Multiple-Valued Log.*, May 2009, pp. 18–23.
- [20] R. Wang, W. Hong, and N. Yang, "The research on footprint recognition method based on wavelet and fuzzy neural network," in *Proc. 9th Int. Conf. Hybrid Intell. Syst.*, Aug. 2009, pp. 428–432.
- [21] V. D. A. Kumar and M. Ramakrishnan, "Footprint recognition using modified sequential haar energy transform (MSHET)," *Int. J. Comput. Sci. Issue*, vol. 7, no. 3, p. 47, 2010.
- [22] A. Kumar and S. Shekhar, "Personal identification using multibiometrics rank-level fusion," *IEEE Trans. Syst., Man, Cybern. C, Appl. Rev.*, vol. 41, no. 5, pp. 743–752, Sep. 2011.
- [23] T. C. Pataky, T. Mu, K. Bosch, D. Rosenbaum, and J. Y. Goulermas, "Gait recognition: Highly unique dynamic plantar pressure patterns among 104 individuals," *J. Roy. Soc. Interface*, vol. 9, no. 69, pp. 790–800, Apr. 2012. [Online]. Available: <http://rsif.royalsocietypublishing.org/content/early/2011/08/31/rsif.2011.0430>
- [24] V. D. A. Kumar and M. Ramakrishnan, "Legacy of footprints recognition—a review," *Int. J. Comput. Appl.*, vol. 35, no. 11, pp. 9–16, 2011.
- [25] V. D. A. Kumar and M. Ramakrishnan, *Footprint Based Recognition System*. Berlin, Germany: Springer, 2011, pp. 358–367.
- [26] V. D. A. Kumar, M. Ramakrishnan, and G. Jagdeesh, "A discrete correlation of footprint image aforementioned to recognition," in *Proc. Nat. Conf. Future Comput.*, Mar. 2012, pp. 5–11.
- [27] V. D. A. Kumar and M. Ramakrishnan, "Manifold feature extraction for foot print image," *Indian J. Bioinf. Biotechnol.*, vol. 1, no. 2, pp. 28–31, 2012. [Online]. Available: <http://ijbb.informaticspublishing.com/index.php/ijbb/article/view/31333>
- [28] K. M. Hashem and F. Ghali, "Human identification using foot features," *Int. J. Eng. Manuf.*, vol. 6, no. 4, pp. 22–31, Jul. 2016.
- [29] G. Qian, J. Zhang, and A. Kidané, *People Identification Using Gait Via Floor Pressure Sensing and Analysis*. Berlin, Germany: Springer, 2008, pp. 83–98, doi: [10.1007/978-3-540-88793-5_7](https://doi.org/10.1007/978-3-540-88793-5_7).
- [30] G. Qian, J. Zhang, and A. Kidane, "People identification using floor pressure sensing and analysis," *IEEE Sensors J.*, vol. 10, no. 9, pp. 1447–1460, Sep. 2010.
- [31] J. Lu and Y.-P. Tan, "Uncorrelated discriminant simplex analysis for view-invariant gait signal computing," *Pattern Recognit. Lett.*, vol. 31, no. 5, pp. 382–393, Apr. 2010. [Online]. Available: <http://www.sciencedirect.com/science/article/pii/S0167865509003092>
- [32] W. Jia, H.-Y. Cai, J. Gui, R.-X. Hu, Y.-K. Lei, and X.-F. Wang, "Newborn footprint recognition using orientation feature," *Neural Comput. Appl.*, vol. 21, no. 8, pp. 1855–1863, Nov. 2012, doi: [10.1007/s00521-011-0530-9](https://doi.org/10.1007/s00521-011-0530-9).
- [33] V. D. A. Kumar, "Footprint recognition with cop using principle component analysis (PCA)," *J. Comput. Inf. Syst.*, vol. 8, no. 12, pp. 4939–4950, 2012.
- [34] V. D. A. Kumar and M. Ramakrishnan, "A comparative study of fuzzy evolutionary techniques for footprint recognition and performance improvement using wavelet-based fuzzy neural network," *Int. J. Comput. Appl. Technol.*, vol. 48, no. 2, pp. 95–105, Aug. 2013, doi: [10.1504/IJCAT.2013.056016](https://doi.org/10.1504/IJCAT.2013.056016).
- [35] V. D. A. Kumar and M. Ramakrishnan, "Manifold feature extraction for foot print image," *Indian J. Comput. Sci. Eng.*, vol. 3, no. 6, pp. 774–778, 2013. [Online]. Available: <http://www.ijcse.com/docs/INDJCSE12-03-06-052.pdf>
- [36] R. Khokher, R. C. Singh, and R. Kumar, "Footprint recognition with principal component analysis and independent component analysis," *Macromolecular Symposia*, vol. 347, no. 1, pp. 16–26, Jan. 2015, doi: [10.1002/masy.201400045](https://doi.org/10.1002/masy.201400045).
- [37] R. Kushwaha and N. Nain, "Person identification using footprint minutiae," in *Proc. 3rd Int. Conf. Comput. Vis. Image Process.*, B. B. Chaudhuri, M. Nakagawa, P. Khanna, and S. Kumar, Eds. Singapore: Springer, 2020, pp. 285–299.
- [38] R. Kushwaha, G. Singal, and N. Nain, "A texture feature based approach for person verification using footprint bio-metric," *Artif. Intell. Rev.*, vol. 2020, pp. 1–31, Aug. 2020. [Online]. Available: <https://link.springer.com/article/10.1007%2Fs10462-020-09887-6>
- [39] K. K. Nagwanshi, "Cyber-forensic review of human footprint and gait for personal identification," *IAENG Int. J. Comput. Sci.*, vol. 46, no. 4, pp. 645–661, 2019, published by IAENG. [Online]. Available: http://www.iaeng.org/IJCS/issues_v46/issue_4/IJCS_46_4_15.pdf
- [40] K. K. Nagwanshi, "Learning classifier system," in *Modern Optimization Methods for Science, Engineering and Technology*. Bristol, U.K.: IOP Publishing, 2019, pp. 1–8, doi: [10.1088/978-0-7503-2404-5ch8](https://doi.org/10.1088/978-0-7503-2404-5ch8).
- [41] M. Alojail and S. Bhatia, "A novel technique for behavioral analytics using ensemble learning algorithms in E-Commerce," *IEEE Access*, vol. 8, pp. 150072–150080, 2020.
- [42] S. Bhatia, P. Chaudhary, and N. Dey, *Opinion Score Mining System*. Singapore: Springer, 2020, pp. 23–34, doi: [10.1007/978-981-15-5043-0_2](https://doi.org/10.1007/978-981-15-5043-0_2).
- [43] A. Gupta and D. Raj, "Novel distance metric for touch less footprint based identification technique," *Int. J. Innov. Technol. Exploring Eng.*, vol. 9, no. 3, pp. 1011–1016, 2020, doi: [10.35940/ijtee.C7967.019320](https://doi.org/10.35940/ijtee.C7967.019320).
- [44] K. K. Nagwanshi and S. Dubey, "Dataset: Biometric 220 × 6 human footprint," *IEEE Dataport*, 2019, doi: [10.21227/7gmx-jq63](https://doi.org/10.21227/7gmx-jq63).
- [45] R. Kumar. (2019). *Footprint Image Database: Dataset of Footprint Images of 21 Individuals*. [Online]. Available: <https://github.com/goodrahstar/footprint-database>
- [46] M. S. Nixon and A. S. Aguado, "6-flexible shape extraction (snakes and other techniques)," in *Feature Extraction and Image Processing*, M. S. Nixon and A. S. Aguado, Eds. Oxford, U.K.: Newnes, 2002, pp. 217–245. [Online]. Available: <http://www.sciencedirect.com/science/article/pii/B9780080506258500109>
- [47] F. Xing and L. Yang, "Machine learning and its application in microscopic image analysis," in *Machine Learning and Medical Imaging*, G. Wu, D. Shen, and M. R. Sabuncu, Eds. New York, NY, USA: Academic, 2016, pp. 97–127. [Online]. Available: <http://www.sciencedirect.com/science/article/pii/B9780128040768000049>
- [48] C. Labno. (2020). *Basic Intensity Quantification With Imagej*. [Online]. Available: <https://www.unige.ch/medecine/bioimaging/files/1914/1208/6000/Quantification.pdf>
- [49] K. K. Nagwanshi and S. Dubey, "Estimation of centroid, ensembles, anomaly and association for the uniqueness of human footprint features," *Int. J. Intell. Eng. Inform.*, vol. 8, no. 2, pp. 117–137, Aug. 2020, doi: [10.1504/IJIEI.2020.109096](https://doi.org/10.1504/IJIEI.2020.109096).
- [50] K. K. Nagwanshi and S. Dubey, "Statistical feature analysis of human footprint for personal identification using BigML and IBM Watson analytics," *Arabian J. Sci. Eng.*, vol. 43, no. 6, pp. 2703–2712, Jun. 2018, doi: [10.1007/s13369-017-2711-z](https://doi.org/10.1007/s13369-017-2711-z).
- [51] X. Liu, M. Song, D. Tao, Z. Liu, L. Zhang, C. Chen, and J. Bu, "Random forest construction with robust semisupervised node splitting," *IEEE Trans. Image Process.*, vol. 24, no. 1, pp. 471–483, Jan. 2015.
- [52] L. Simon. (2019). *Probability Theory and Mathematical Statistics (Stat 414 / 415): Lesson 54: Power of a Statistical Test: Calculating Sample Size*. [Online]. Available: <https://newonlinecourses.science.psu.edu/stat414/node/306/>
- [53] S. Theodoridis and K. Koutroubas, "Supervised learning: The epilogue," in *Pattern Recognition*, 4th ed, S. Theodoridis and K. Koutroubas, Eds. Boston, MA, USA: Academic, 2009, pp. 567–594. [Online]. Available: <http://www.sciencedirect.com/science/article/pii/B9781597492720500128>
- [54] L. A. Zadeh, "Fuzzy sets," *Inf. Control*, vol. 8, no. 3, pp. 338–353, Jun. 1965. [Online]. Available: <http://www.sciencedirect.com/science/article/pii/S00199586590241X>
- [55] L. A. Zadeh, "Fuzzy logic," *Computer*, vol. 21, no. 4, pp. 83–93, Apr. 1988.
- [56] E. H. Mamdani and S. Assilian, "An experiment in linguistic synthesis with a fuzzy logic controller," *Int. J. Man-Mach. Stud.*, vol. 7, no. 1, pp. 1–13, Jan. 1975. [Online]. Available: <http://www.sciencedirect.com/science/article/pii/S0020737375800022>

- [57] T. Takagi and M. Sugeno, "Fuzzy identification of systems and its applications to modeling and control," *IEEE Trans. Syst., Man, Cybern.*, vol. SMC-15, no. 1, pp. 116–132, Jan. 1985.
- [58] H.-S. Lim, "An improved kNN learning based korean text classifier with heuristic information," in *Proc. 9th Int. Conf. Neural Inf. Process. ICONIP*, Nov. 2002, pp. 731–735.



SHAKILA BASHEER is currently an Assistant Professor with the Department of Information Systems, College of Computer and Information Sciences, Princess Nourah bint Abdulrahman University, Riyadh, Saudi Arabia. She has more than ten years of teaching experience and has published more technical papers in international journals/proceedings of international conferences/ edited chapters of reputed publications. She has worked and contributed in the field of data mining, image processing, and fuzzy logic. Her research also focuses on data mining algorithms using fuzzy logic. She is currently working on data mining, vehicular networks machine learning, block chain, vehicular networks, and the IoT.



KAPIL KUMAR NAGWANSHI (Senior Member, IEEE) received the B.Eng. degree (Hons.) from Guru Ghasidas Central University, Bilaspur, in 2001, and the M.Eng. degree in computer technology and application and the Ph.D. degree from Chhattisgarh Swami Vivekanand Technical University (CSVTU) Bhilai, in 2008 and 2019, respectively. He is currently an Associate Professor with ASET Amity University Rajasthan, Jaipur, India. His primary domain of teaching and research includes the Internet of Things, digital image processing, cyber forensics, data science and engineering, AI, and computer networking.



SURBHI BHATIA received the Ph.D. degree in computer science and engineering from Banasthali Vidyapeeth, India. She is currently an Assistant Professor with the Department of Information Systems, College of Computer Sciences and Information Technology, King Faisal University, Saudi Arabia. She has rich eight years of teaching and academic experience. She is in the Editorial board member with Inderscience Publishers in *International Journal of Hybrid Intelligence*, *SN Applied Sciences*, Springer and also in several IEEE conferences. She has published seven national and international patents. She has published more than 30 papers in reputed journals and conferences in high indexing databases. She is currently serving as a guest editor of special issues in reputed journals. She has delivered talks as keynote speaker in IEEE conferences and in faculty development programs. She has successfully authored two books from Springer and Wiley. She is currently editing three books from CRC Press, Elsevier and Springer. She has been an active researcher in the field of data mining, machine learning, and information retrieval.



SIPI DUBEY received the Ph.D. degree in computer science and engineering from CSVTU, Bhilai, in 2010. She is currently working as a Professor with the Rungta College of Engineering and Technology, (RCET) Bhilai, C.G. Her research interest is image processing. She has more than 60 publications in reputed international journals and conferences.



G. R. SINHA (Senior Member, IEEE) received the Ph.D. degree. He is currently an Adjunct Professor with the International Institute of Information Technology Bangalore (IIITB) and currently deputed as a Professor with the Myanmar Institute of Information Technology (MIIT), Mandalay, Myanmar. He is a Visiting Professor (Honorary) with Sri Lanka Technological Campus Colombo for one year, from 2019 to 2020. He has more than 200 research papers, edited books, and books into his credit. He has edited books for reputed International publishers. He has teaching and research experience of 21 years. He has been the Dean of Faculty and an Executive Council Member of CSVTU and currently a member of Senate of MIIT. He has been delivering ACM lectures as a ACM Distinguished Speaker in the field of DSP, since 2017, across the world. His research interests include biometrics, cognitive science, medical image processing, computer vision, outcome based education (OBE), and ICT tools for developing Employability Skills. He is a Fellow of the Institute of Engineers India and a Fellow of IETE, India. He served as a Distinguished IEEE Lecturer in IEEE India council for Bombay section. He was a recipient of many awards and recognitions at national and international level. He has delivered more than 50 Keynote/Invited Talks and Chaired many Technical Sessions in International Conferences across the world. He has eight Ph.D. Scholars, 15 M.Tech. Scholars, and has been Supervising one Ph.D. Scholar. He is active reviewer and editorial member of more than 12 reputed International journals in his research areas, such as IEEE Transactions, Elsevier journals, and Springer journals.

...